# REPORT DOCUMENTATION PAGE

Form Approved OMB NO. 0704-0188



| 1. REPORT DATE (DD-MM-YYYY) | 2. REPORT TYPE | 3. DATES COVERED (From - To) |
|---|---|---|
| 23-03-2011 | Final Report | 1-Sep-2009 - 31-Jul-2010 |

4. TITLE AND SUBTITLE

Electro-Thermo-Mechanical Homogenization of Ferroelectric Atomistic Medium

5a. CONTRACT NUMBER
W911NF-09-1-0443

5b. GRANT NUMBER

5c. PROGRAM ELEMENT NUMBER
665803

6. AUTHORS
Jacob Fish

5d. PROJECT NUMBER

5e. TASK NUMBER

5f. WORK UNIT NUMBER

7. PERFORMING ORGANIZATION NAMES AND ADDRESSES
Rensselaer Polytechnic Institute
Office of Sponsored Research
Rensselaer Polytechnic Institute
Troy, NY 12180 -

8. PERFORMING ORGANIZATION REPORT NUMBER

9. SPONSORING/MONITORING AGENCY NAME(S) AND ADDRESS(ES)
U.S. Army Research Office
P.O. Box 12211
Research Triangle Park, NC 27709-2211

10. SPONSOR/MONITOR'S ACRONYM(S)
ARO

11. SPONSOR/MONITOR'S REPORT NUMBER(S)
56102-EG.1

12. DISTRIBUTION AVAILIBILITY STATEMENT
Approved for Public Release; Distribution Unlimited

13. SUPPLEMENTARY NOTES
The views, opinions and/or findings contained in this report are those of the author(s) and should not contrued as an official Department of the Army position, policy or decision, unless so designated by other documentation.

14. ABSTRACT
Two-scale continuum equations are derived for heterogeneous continua with full nonlinear electromechanical coupling using nonlinear mathematical homogenization theory. The resulting coarse-scale electromechanical continuum equations are free of coarse-scale constitutive equations. The unit cell (or Representative Volume Element) is subjected to the overall mechanical and electric fields extracted from the solution of the coarse-scale problem and is solved for arbitrary constitutive equations of fine-scale constituents. The proposed method can be

15. SUBJECT TERMS
electroactive, multiscale, homogenization, electromechanical coupling, unit cell,

| 16. SECURITY CLASSIFICATION OF: | | | 17. LIMITATION OF ABSTRACT | 15. NUMBER OF PAGES | 19a. NAME OF RESPONSIBLE PERSON |
|---|---|---|---|---|---|
| a. REPORT | b. ABSTRACT | c. THIS PAGE | | | Jacob Fish |
| UU | UU | UU | UU | | 19b. TELEPHONE NUMBER 212-854-5275 |

**Report Title**


## ABSTRACT

Two-scale continuum equations are derived for heterogeneous continua with full nonlinear electromechanical coupling using nonlinear mathematical homogenization theory. The resulting coarse-scale electromechanical continuum equations are free of coarse-scale constitutive equations. The unit cell (or Representative Volume Element) is subjected to the overall mechanical and electric fields extracted from the solution of the coarse-scale problem and is solved for arbitrary constitutive equations of fine-scale constituents. The proposed method can be applied to simulate the behavior of electroactive materials with heterogeneous fine-scale structure and design new electroactive materials and devices.


## List of papers submitted or published that acknowledge ARO support during this reporting period. List the papers, including journal references, in the following categories:

### (a) Papers published in peer-reviewed journals (N/A for none)

**Number of Papers published in peer-reviewed journals:** 0.00

### (b) Papers published in non-peer-reviewed journals or in conference proceedings (N/A for none)

**Number of Papers published in non peer-reviewed journals:** 0.00

### (c) Presentations

**Number of Presentations:** 0.00

### Non Peer-Reviewed Conference Proceeding publications (other than abstracts):

**Number of Non Peer-Reviewed Conference Proceeding publications (other than abstracts):** 0

### Peer-Reviewed Conference Proceeding publications (other than abstracts):

**Number of Peer-Reviewed Conference Proceeding publications (other than abstracts):** 0

### (d) Manuscripts

**Number of Manuscripts:** 0.00

### Patents Submitted

### Patents Awarded

## Awards

### Graduate Students

| NAME | PERCENT_SUPPORTED |
|---|---|
| **FTE Equivalent:** | |
| **Total Number:** | |

### Names of Post Doctorates

| NAME | PERCENT_SUPPORTED |
|---|---|
| **FTE Equivalent:** | |
| **Total Number:** | |

### Names of Faculty Supported

| NAME | PERCENT_SUPPORTED | National Academy Member |
|---|---|---|
| Jacob Fish | 0.03 | No |
| Sergey Kuznetsov | 0.30 | No |
| **FTE Equivalent:** | **0.33** | |
| **Total Number:** | **2** | |

### Names of Under Graduate students supported

| NAME | PERCENT_SUPPORTED |
|---|---|
| **FTE Equivalent:** | |
| **Total Number:** | |

### Student Metrics

This section only applies to graduating undergraduates supported by this agreement in this reporting period

The number of undergraduates funded by this agreement who graduated during this period: .....

The number of undergraduates funded by this agreement who graduated during this period with a degree in science, mathematics, engineering, or technology fields:.....

The number of undergraduates funded by your agreement who graduated during this period and will continue to pursue a graduate or Ph.D. degree in science, mathematics, engineering, or technology fields:.....

Number of graduating undergraduates who achieved a 3.5 GPA to 4.0 (4.0 max scale): .....

Number of graduating undergraduates funded by a DoD funded Center of Excellence grant for Education, Research and Engineering: .....

The number of undergraduates funded by your agreement who graduated during this period and intend to work for the Department of Defense .....

The number of undergraduates funded by your agreement who graduated during this period and will receive scholarships or fellowships for further studies in science, mathematics, engineering or technology fields: .....

### Names of Personnel receiving masters degrees

| NAME |
| --- |
| **Total Number:** |

## Names of personnel receiving PHDs

| NAME |
| --- |
| **Total Number:** |

## Names of other research staff

| NAME | PERCENT_SUPPORTED |
| --- | --- |
| **FTE Equivalent:** | |
| **Total Number:** | |

## Sub Contractors (DD882)

## Inventions (DD882)

## Scientific Progress

The examples considered in this report show that nonlinear mathematical homogenization captures well the coarse-scale behavior of heterogeneous electroactive composite and its dependence on the fine-scale details.
At the same time the method shares the shortcomings common to the first order homogenization methods; it is insensitive to the absolute size of the UC because of assumption of UC infinitesimality. This lack of accuracy increases with the unit cell size and the magnitude of strains and electric fields inhomogeneities.
In future we plan to study mathematical homogenization for various dynamic problems. In particular of interest are studies of wave propagation in the media with periodic resonant structures. It would be interesting to explore if mathematical homogenization can capture the negative effective refractive indexes as it was found in metamaterials. Can this framework be used to control bandgaps by biasing fields and will it allow extending effective bandgaps for use in various devices (for subwavelength imaging, wave attenuation etc). The other interesting phenomenon, which possibly may be studied using mathematical homogenization is the controlled response of smart structures to various impacts. Depending on the impact a control strategy may be developed to obtain the desired response from the smart structure. This phenomenon might be utilized in development of smart armor and other structures. Fine-scale structure optimization aimed at optimizing coarse-scale properties, in particular for electroactive polymers containing composites, is another useful application of the method. The asymptotic expansion would allow to isolate the term , responsible for electrostrictive and electrostatic coupling. Making this term larger will permit increasing the actuation.

## Technology Transfer

Non

# Electro-Thermo-Mechanical Homogenization of Ferroelectric Atomistic Medium

**PI: Jacob Fish**

**Program Monitor: Bruce LaMattina**

# Final Report

**Summary**

Two-scale continuum equations are derived for heterogeneous continua with full nonlinear electromechanical coupling using *nonlinear mathematical homogenization* theory. The resulting coarse-scale electromechanical continuum equations are free of coarse-scale constitutive equations. The unit cell (or Representative Volume Element) is subjected to the overall mechanical and electric fields extracted from the solution of the coarse-scale problem and is solved for arbitrary constitutive equations of fine-scale constituents. The proposed method can be applied to simulate the behavior of electroactive materials with heterogeneous fine-scale structure and design new electroactive materials and devices.

**Keywords:** electroactive, multiscale, homogenization, electromechanical coupling, unit cell, electostriction, composite, polycrystalline, fine-scale structure.

## 1. Introduction

All industrial materials are heterogeneous at some scale. The overall behavior of materials is controlled by their fine-scale structure and materials with tunable fine-scale structure can exhibit superior performance at coarse level. Multiphase fine-scale structure allows improving useful properties while reducing the effect of undesirable properties of fine-scale constituents. The overall properties can be tailored by changing fine-scale structure (mixing different materials at different scales, changing the size and shape of constituents, etc) to meet the needs of specific applications. Attempts have even been made to state an optimization problem aimed at constructing an optimal material architecture [1,2,3,4,5,6,7,8]. Due to the synergy of fine-scale constituents it is possible to obtain new properties which are not available in fine-scale constituents alone. Metamaterials [9,10,11,12,13] represent one fascinating example of how tuning fine-scale structure provides a completely different dynamic behavior of materials.

Historically, the primary goal of composite materials with tunable fine-scale structure was to reduce weight in particular in aerospace applications. More recently, emphasis has been placed on electroactive materials, which found their use in actuators, transducers and structures capable of changing their properties (behavior) depending on the environment. These are so-called “smart

structures" where feedback loop comprises of sensors and actuators. The presence of biasing fields makes such materials apparently behave differently [14,15]**,** which creates an opportunity to control the response of so-called smart structures to various excitations. Electroactive materials are used for actuators, sensors and smart structures. Applications range but not limited to underwater acoustics, biomedical imaging [16], robotic manipulations, artificial muscles [17,18,19], active damping, resonators and filters for frequency control and selection for telecommunication, precise timing and synchronization[14], MEM and NEM devices [20,21,22], flow control [23], precise positioning [24, 25], conformal control surfaces [26], power electronic devices [27], computer memory applications [21,22], tunable optics, generators for harvesting energy, tactile sensors [28,29,30,31], etc.

Composites, combining electroactive materials with other materials, allow to overcome the limitations intrinsic to pure electroactive materials such as low actuation capabilities, high electric fields, fast decay and instabilities. The overall properties of such composites are extremely sensitive to fine-scale details. Various studies [19,26,32,33,34,35] have shown that electromechanical coupling can be significantly improved by making non-homogeneous electromechanical actuators, composites of flexible and high dielectric modulus or even conductive materials. The overall response of a composite actuator can be vastly superior to that of its constituents. In particular, composites based on electroactive polymers have shown tremendous promise due to their actuation capabilities resulting from the ability to produce strains of up to 40% [28,26], and more than 100% in elastomer actuation [36]. The attractiveness of polymers is not only due to their electromechanical properties, but also due to their lightweight, short response time, low noise, durability and high specific energy. Proper optimization of their fine-scale structure can lead to a vast improvement in electromechanical coupling [26].

On the modeling front, there are numerous nonlinear models [37,14, 38,39,40,41,42,43,44,45,46, 47,48,49] capable of describing electromechanical behavior for large deformation problems. There are a number of constitutive phenomenological and micromechanical models for electromechanical materials, such as ferroelectric switching [50,51,52,53,54,55]. So while the behavior of different phases is well understood and can be described sufficiently well, the computational cost of resolving fine-scale details is very high and is often beyond the capacity of modern computers. Thus models capable of describing the overall behavior of electroactive composites without resolving fine-scale details are needed. The phenomenological equations describing the behavior of electroactive composites are usually very complex and often unknown and thus there is increasing need for multiscale-multiphysics based methods.

There are a number of publications which make use of homogenization theory for electromechanical coupling in composites and polycrystalline materials, but mostly restricted to linear piezoelectric coupling [1,8,56,57,58,59,60,61,62,63]. For mechanical problems a number of homogenization methods accounting for large deformations and arbitrary nonlinear constitutive relations have been developed [64,65,66,67,68,69,70,71,72]. In the present manuscript we extend the nonlinear homogenization framework proposed in [65] to nonlinear electromechanical

materials. To the authors' knowledge this is first attempt to develop a general nonlinear mathematical homogenization theory for electromechanical materials. The derivations of this paper are applicable to arbitrary fine-scale structures and arbitrary constitutive models of phases.

## 2. Mathematical model

First we present the equations describing the behavior of a deformable-polarizable body, subjected to mechanical and electrical excitations. The formulation follows the works of Yang and Tiersten [37,14]. The approach is based on full electromechanical coupling in a solid via Maxwell stress, general nonlinear constitutive equations, large deformations and strong electric fields. Quasistatic approximation is adopted.

Consider deformable-polarizable body occupying volume $\Omega$ with boundary $\partial\Omega$. When the body is placed in electric field, differential material elements experience both body forces and couples due to electric field. There is a full coupling through the Maxwell stress and via the constitutive equations [14,50]. Following Tiersten [37], the electric body force $\mathbf{F}^E$, couple $\mathbf{C}^E$ and power $w^E$ are used to derive the balance equations

$$F_j^E = \rho_e E_j + P_i E_{j,i}, \tag{2.1}$$

$$C_i^E = \varepsilon_{ijk} P_j E_k, \tag{2.2}$$

$$w^E = \rho_m E_i \dot{\pi}_i, \tag{2.3}$$

where $E_j$ denotes electric field, $\rho_m$ the current mass density, $\rho_e$ the current free charge density and $\pi = P_i / \rho_x$ the polarization per unit mass. From (2.1) and (2.2), the governing equations can be derived following [14,37]:

Gauss law

$$D_{i,i} - \rho_e = 0, \tag{2.4}$$

where $D_i$ denotes the electric displacement,

$$D_i = \varepsilon_0 E_i + P_i, \tag{2.5}$$

$P_i$ and $\varepsilon_0$ are polarization and electric constant, respectively. Since divergence of polarization determines induced charge density, the total charge density is given by

$$\rho_e^t = \rho_e - P_{i,i}. \tag{2.6}$$

The electric field is vortex free which can be written as

$$\varepsilon_{ijk} E_{k,j} = 0, \tag{2.7}$$

which implies that electric field can be expressed in terms of the gradient of electric potential

$$E_i = -\phi_{,i}. \tag{2.8}$$

The continuity equation is given by

$$\dot{\rho}_m + \rho_m v_{i,i} = 0 \tag{2.9}$$

and the linear momentum balance equation is

$$\sigma_{ij,j} + \rho_m b_i + F_i^E = \left(\sigma_{ij,j} + \sigma_{ij,j}^E\right) + b_i = \rho_m \dot{v}_i, \tag{2.10}$$

where $\sigma_{ij}$ is Cauchy stress, $b_i$ the body force (excluding electric body force); $\sigma_{ij}^E$ is electrostatic stress, which is related to electric force $\sigma_{ij,j}^E = F_i^E$.

The electrostatic stress $\sigma_{ij}^E$ can be expressed as

$$\sigma_{ij}^E = D_i E_j - \frac{1}{2}\varepsilon_0 E_k E_k \delta_{ij} = P_i E_j + \varepsilon_0 \left( E_i E_j - \frac{1}{2} E_k E_k \delta_{ij} \right) \tag{2.11}$$

Divergence of $\sigma_{ij}^E$ is given by

$$\sigma_{ij,j}^E = D_{j,j} E_i + P_j E_{i,j} = \rho_e E_i + P_j E_{i,j} = F_i^E. \tag{2.12}$$

The sum of Cauchy stress $\sigma_{ij}$ and the electrostatic stress $\sigma_{ij}^E$ gives the total stress $\tau_{ij} = \sigma_{ij} + \sigma_{ij}^E$, which is symmetric and can be decomposed into symmetric tensor

$$\sigma_{ij}^S = \sigma_{ij} + P_i E_j = \sigma_{ji}^S \tag{2.13}$$

and Maxwell stress tensor

$$\sigma_{ij}^M = \varepsilon_0 \left( E_i E_j - \frac{1}{2} E_k E_k \delta_{ij} \right) = \sigma_{ji}^M. \tag{2.14}$$

Using the total stress, the balance of linear momentum (2.10) can be rewritten as

$$\tau_{ij,j} + \rho_m b_i = \rho_m \dot{v}_i. \tag{2.15}$$

The angular momentum balance equation is given by

$$\varepsilon_{ijk} \sigma_{jk} + C_i^E = \varepsilon_{ijk} \left( \sigma_{jk} + P_j E_k \right) = \varepsilon_{ijk} \left( \sigma_{jk} + \sigma_{jk}^E \right) = 0, \tag{2.16}$$

or

$$\varepsilon_{ijk}\tau_{jk} = 0, \tag{2.17}$$

which suggests that the total stress is symmetric.

The conservation of energy is given by

$$\rho_m \dot{e} = \sigma_{ij} v_{i,j} + \rho_m E_i \dot{\pi}_i. \tag{2.18}$$

The free energy can be introduced through Legendre transform

$$\psi = e - E_i P_i, \tag{2.19}$$

and

$$\rho_m \dot{\psi} = \sigma_{ij} v_{i,j} - P_i \dot{E}_i. \tag{2.20}$$

The free energy provides the constitutive relations

$$P_i = P_i\left(E_j, \varepsilon_{kj}\right), \tag{2.21}$$

$$\sigma_{ij} = \sigma_{ij}\left(E_k, \varepsilon_{kl}\right). \tag{2.22}$$

In the present manuscript the weak form of governing equations will be expressed in the initial configuration. Therefore, we will transform the strong form of governing equations into the initial configuration. The balance laws in the so-called in Lagrangian description are given by

$$\mathcal{D}_{J,J} - \rho_E = 0, \tag{2.23}$$

where $\mathcal{D}_L = JF^{-1}_{L,i} D_i$ and $\rho_E = \rho_e J$ are Lagrangian description of electric displacement and charge density, $D_i = J^{-1} F_{i,L} \mathcal{D}_L$.

Electric field is vortex free in the Lagrangian description and is given by

$$\varepsilon_{IJK} \mathcal{E}_{K,J} = 0, \tag{2.24}$$

where $\mathcal{E}_K = E_i F_{i,K} = -\phi_{,i} F_{i,K} = -\phi_{,K}$ is Lagrangian description of electric field, $E_i = \mathcal{E}_K F^{-1}_{K,i}$. Equation (2.24) can be used implicitly to describe electric field as a gradient of electric potential.

$$K_{kL,L} + B_k = \rho_M \dot{v}_k, \tag{2.25}$$

where $K_{iL} = JF^{-1}_{L,j}\tau_{ij}$ and $\rho_M = \rho_m J$ are the first Piola-Kirchhoff stress and material density, respectively, and $\tau_{ij} = J^{-1} F_{j,L} K_{iL}$. $K_{iL}$ is nonsymmetric satisfying

$$\varepsilon_{kij} F_{j,L} K_{iL} = 0, \tag{2.26}$$

which confirms that moments resulting from electric body force acting on the infinitesimal volume are equilibrated by internal forces.
The energy balance equation is given by

$$\rho_M \dot{\psi} = T_{KL}^S \dot{S}_{KL} - \mathcal{P}_K \dot{\mathcal{E}}_K, \tag{2.27}$$

where the second Piola-Kirchhoff stress $T_{KL}^S$ is

$$T_{KL}^S = JF_{K,k}^{-1} F_{L,l}^{-1} \sigma_{kl}^S. \tag{2.28}$$

The Green-Lagrange strain is given by

$$S_{KL} = \left( u_{K,L} + u_{L,K} + u_{M,K} u_{M,L} \right) / 2 \tag{2.29}$$

and the Lagrangian description of polarization vector $\mathcal{P}_K$ is

$$\mathcal{P}_K = JF_{K,k}^{-1} P_k, \;\; P_i = J^{-1} F_{i,K} \mathcal{P}_K, \tag{2.30}$$

$$\sigma_{ij}^S = \sigma_{ij} + P_i E_j = J^{-1} F_{i,K} F_{i,L} T_{KL}^S. \tag{2.31}$$

The energy balance determines constitutive equations, which can be written as

$$\begin{aligned} T_{KL}^S &= T_{KL}^S \left( S_{KL}, \mathcal{E}_K \right) = \rho_M \frac{\partial \psi}{\partial S_{KL}}, \\ \mathcal{P}_K &= \mathcal{P}_K \left( S_{KL}, \mathcal{E}_K \right) = -\rho_M \frac{\partial \psi}{\partial \mathcal{E}_K}. \end{aligned} \tag{2.32}$$

$K_{iL}$ and $\mathcal{D}_L$ may be calculated from

$$\begin{aligned} K_{jL} &= F_{j,K} \rho_M \frac{\partial \psi}{\partial S_{KL}} + JF_{i,L} \varepsilon_0 \left( E_i E_j - \frac{1}{2} E_k E_k \delta_{ij} \right), \\ \mathcal{D}_K &= \varepsilon_0 J C_{KL}^{-1} \mathcal{E}_L - \rho_M \frac{\partial \psi}{\partial \mathcal{E}_K}. \end{aligned} \tag{2.33}$$

To complete the strong form (2.23), (2.25), (2.32), (2.33) of the initial-boundary value problem is given by

$$\begin{aligned} &u_i = \bar{u}_i \quad on \quad \partial\Omega^u, \\ &\varphi = \bar{\varphi} \quad on \quad \partial\Omega^\varphi, \\ &K_{kL} N_L = \bar{T}_K \quad on \quad \partial\Omega^T, \\ &\bar{D}_K N_K = -\bar{\omega} \quad on \quad \partial\Omega^\omega, \\ &u_i = \bar{u}_i(0) \quad at \quad t = 0, \\ &\frac{\partial u_i}{\partial t} = \bar{v}_i(0), \end{aligned} \tag{2.34}$$

where $\bar{\omega}$ is surface charge density applied on the portion of the surface $\partial\Omega^{\omega}$ and $\bar{T}_K$ is mechanical traction applied on the portion of the surface $\partial\Omega^{T}$; $\bar{u}_i$ and $\bar{\varphi}$ are displacements and electric potential prescribed on the surfaces $\partial\Omega^{u}$ and $\partial\Omega^{\varphi}$, respectively, such that

$$\begin{aligned} \partial\Omega^{\omega} \cap \partial\Omega^{\varphi} &= \partial\Omega^{u} \cap \partial\Omega^{T} = \partial\Omega \\ \partial\Omega^{\omega} \cup \partial\Omega^{\varphi} &= \partial\Omega^{u} \cup \partial\Omega^{T} = 0 \end{aligned} \tag{2.35}$$

The free energy, which determines constitutive relationships for nonlinear electroelastic materials, can be written as power series of $S_{AB}$ and $\mathcal{E}_A$ [14]

$$\begin{aligned} &\rho_M \psi\left(S_{KL}, \mathcal{E}_K\right) = \frac{1}{2} c_{2ABCD} S_{AB} S_{SD} - e_{ABC} \mathcal{E}_A S_{BC} - \frac{1}{2} \chi_{2AB} \mathcal{E}_A \mathcal{E}_B + \frac{1}{6} c_{3ABCDEF} S_{AB} S_{CD} S_{EF} + \\ &+ \frac{1}{2} k_{ABCDE} \mathcal{E}_A S_{BC} S_{DE} - \frac{1}{2} b_{ABCD} \mathcal{E}_A \mathcal{E}_B S_{CD} - \frac{1}{6} \chi_{3ABC} \mathcal{E}_A \mathcal{E}_B \mathcal{E}_C + \frac{1}{24} c_{4ABCDEFGH} S_{AB} S_{CD} S_{EF} S_{GH} + \\ &+ \frac{1}{6} k_{2ABCDEFG} \mathcal{E}_A S_{BC} S_{DE} S_{FG} + \frac{1}{4} a_{1ABCDEF} \mathcal{E}_A \mathcal{E}_B S_{CD} S_{EF} + \frac{1}{6} k_{3ABCDE} \mathcal{E}_A \mathcal{E}_B \mathcal{E}_C S_{DE} - \frac{1}{4} \chi_{4ABCD} \mathcal{E}_A \mathcal{E}_B \mathcal{E}_C \mathcal{E}_D \end{aligned} \tag{2.36}$$

where constants $c_{2ABCD}$, $e_{ABC}$, $\chi_{2AB}$, $c_{3ABCDEF}$, $k_{ABCDE}$, $b_{ABCD}$, $\chi_{3ABC}$, $c_{4ABCDEFGH}$, $k_{2ABCDEFG}$, $a_{1ABCDEF}$, $k_{3ABCDE}$ $\chi_{4ABCD}$ are often referred to as the fundamental material constants. The structure of $\psi\left(S_{KL}, \mathcal{E}_K\right)$ depends on the symmetries of particular materials under consideration [73,74].

From the above strong form (2.34) it follows that the electric fields, $\boldsymbol{\mathcal{E}}$ and $\boldsymbol{\mathcal{P}}$, are coupled to the mechanical fields, $\mathbf{F}$ and $\mathbf{K}$, at two levels [50]. First, is the *electrostatic* coupling, when the electric fields directly generate distributed forces via Maxwell stress, which in turn affects the mechanical equilibrium of a solid. The resulting stresses depend on the second order terms of electric field, and while typically very small ($10^{-5}$ MPa for a lMV/m field), could have a significant effect if the fluctuations of the electric field are large (field singularities) as in the case of heterogeneous media with high contrast in the dielectric moduli or in electrodes and conducting crack tips [75,76,26]. This nonlinear phenomena is universal and common for both, dielectrics and conductors [77], and has no converse effects, since the mechanical stress state does not directly influence the electrostatic balance [50], but can affect it through the motion, when such a motion changes electric field.

The second level of coupling occurs in the constitutive behavior of dielectric materials, expressed by equations (2.21), (2.22) or (2.32), (2.33). Polarization induces strain, while mechanical stress affects polarization, which introduces full coupling. Most common electromechanical materials are piezoelectrics, ferroelectrics and electrostrictors [78].

In piezoelectrics, there is a linear dependence between applied stress and induced electric displacement (direct piezoelectric effect)

$$D_i = d_{ijk} \sigma_{jk} \tag{2.37}$$

and between applied electric field and induced strain (inverse piezoelectric effect),

$$\varepsilon_{ij} = d_{kij} E_k, \tag{2.38}$$

where $d_{ijk}$ are piezoelectric coefficients. A positive electric field results in positive strain, and vice versa, negative electric field results in negative strain.

Ferroelectric materials have spontaneous polarization $P_s$ in absence of external electric field. The charge due to spontaneous polarization is usually masked by the charges from surroundings of the material. Direction of spontaneous polarization can be switched by external electric field. Thus ferroelectric polycrystallines are characterized by hysteresis in polarization-electric field $\boldsymbol{P(E)}$ and induced strain-electric field $\boldsymbol{\varepsilon(E)}$.

In electrostrictive materials induced strain is proportional to the square of polarization

$$\varepsilon_{ij} = Q_{ijkl} P_k P_l, \tag{2.39}$$

where $Q_{ijkl}$ are electrostrictive coefficients. For mildly strong electric fields, the dependence between polarization and electric field is linear and (2.39) may be written as

$$\varepsilon_{ij} = M_{ijkl} E_k E_l, \tag{2.40}$$

where $M_{ijkl}=\chi_{km}\chi_{ln}Q_{kmln}$ and $\chi_{ij}$ is dielectric susceptibility. Formulation of 'converse' electrostrictive effect is also possible [79]. Here both, positive and negative electric fields result in positive longitudinal strain.

In both, electrostriction and electrostatic coupling the overall behavior is determined by the average of the fluctuation of the electric field (rather than its average). Therefore one can obtain large coupling with relatively small macroscopic field [19,35]. Huang et al. [35] described a three-phase polymer based actuator with more than 8% actuation strain attained with an activation field of 20 MV/m.

## 3. **Mathematical homogenization for nonlinear coupled electromechanical problem**

In this section we will introduce scale separation and proceed with deriving equations for different scales from the strong governing equations in the Lagrangian description derived in the previous section.

Consider a body with volume $\Omega^\lambda$ and surface $\partial\Omega^\lambda$ made of heterogeneous solid with characteristic size of the heterogeneity $l$ which is much smaller than the body dimension so that heterogeneities are considered to be "invisible". The body is effectively homogeneous at the coarse scale; its fine-scale structure can be observed by zooming (Figure 1) at any coarse-scale point $A$. We will denote the volume and boundary of the body on the coarse-scale by $\Omega$ and $\partial\Omega$, respectively.

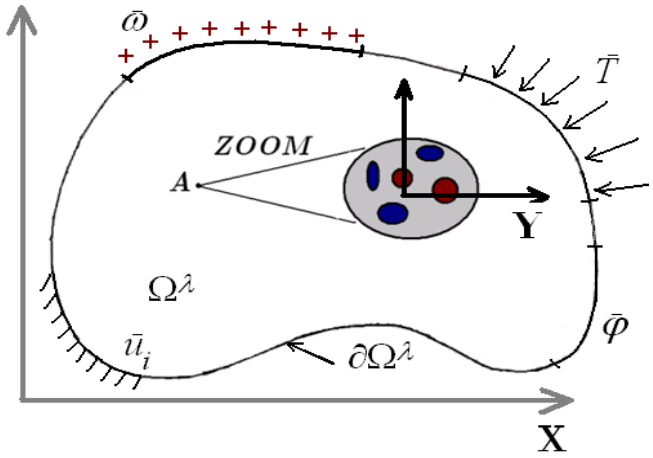


Figure 1. A body with fine-scale heterogeneities

To describe the dependence of various fields $\Psi^\lambda(\mathbf{X})$ on the coarse-scale and fine-scale coordinates we will introduce global coordinate system **X** and local (unit cell) coordinate system **Y** associated with fine-scale structure placed at every coarse-scale point. The two coordinates are related by $\mathbf{Y} = \mathbf{X}/\lambda$, $0 < \lambda \ll 1$. Dependence of the field $\Psi^\lambda(\mathbf{X})$ on the two scale coordinates is denoted as

$$\Psi^\lambda(\mathbf{X}) = \Psi(\mathbf{X}, \mathbf{Y}) \tag{3.1}$$

where superscript $\lambda$ denotes existence fine-scale details.

We assume that the body is composed of a periodic repetition of unit cells (UC) with volume $\Theta_Y$. The periodicity may be global, when the whole body is a lattice consisting of unit cells $\Theta_Y$ (Figure 2.a), or local, when periodicity holds only in a small neighborhood of coarse-scale point (Figure 2.b). Unit cell coordinates **Y** in (3.1) are defined with respect to the initial (undeformed) fine-scale configuration.

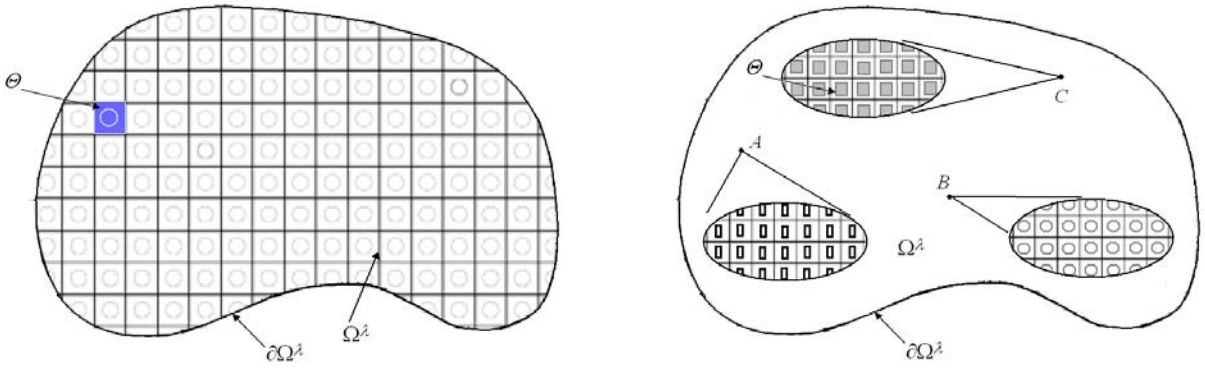


(a) (b)

Figure 2. Global (a) and local (b) periodicity.

To construct the weak form of the governing equations we will need to integrate over the volume $\Omega^\lambda$. This can be carried out as long as the size of unit cell is infinitesimally small, which yields the following fundamental lemma of homogenization ([80,81]

$$\lim_{\lambda\to 0^+}\int_{\Omega^\lambda}\Psi\left(\mathbf{X},\mathbf{Y}\right)d\Omega=\lim_{\lambda\to 0^+}\int_{\Omega}\left(\frac{1}{\left|\Theta_Y\right|}\int_{\Theta_Y}\Psi\left(\mathbf{X},\mathbf{Y}\right)d\Theta\right)d\Omega, \tag{3.2}$$

which also implies that the fine-scale domain $\Theta_Y$ exists at every point in the coarse-scale domain (Figure 3.).

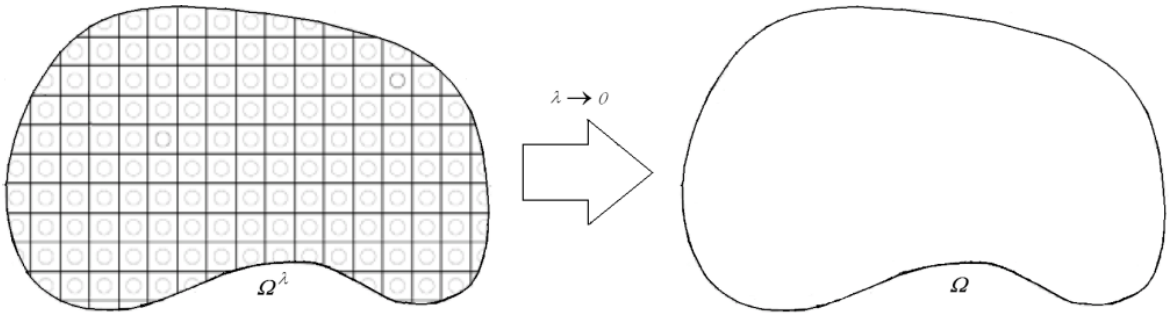


Figure 3. Transition from the heterogeneous to homogeneous domain as $\lambda \to 0^+$

To derive the coarse-scale equations we will start from the equilibrium equation and Gauss law in the Lagrangian description (2.23), (2.25). As before superscript $\lambda$ denotes dependence of a quantity on fine-scale details

$$K^\lambda_{kL,L}\left(F^\lambda,\mathcal{E}^\lambda\right)+B^\lambda_k\left(\mathbf{X}\right)=\rho^\lambda_M\dot{v}, \tag{3.3}$$

$$\mathcal{D}^\lambda_{J,J}\left(F^\lambda,\mathcal{E}^\lambda\right)-\rho^\lambda_E\left(\mathbf{X}\right)=0 \tag{3.4}$$

with initial and boundary conditions

$$\begin{aligned}
&u_i=\bar{u}_i \quad on \quad \partial\Omega^u,\\
&\varphi=\bar{\varphi} \quad on \quad \partial\Omega^\varphi,\\
&K_{kL}N_L=\bar{T}_K \quad on \quad \partial\Omega^T,\\
&\bar{D}_K N_K=-\bar{\omega} \quad on \quad \partial\Omega^\omega,\\
&u^\lambda_i=\bar{u}_i\left(0\right) \quad at \quad t=0,\\
&\frac{\partial u^\lambda_i}{\partial t}=\bar{v}_i\left(0\right) \quad at \quad t=0,
\end{aligned} \tag{3.5}$$

$$\begin{aligned}\partial\Omega^{\lambda\omega}\cap\partial\Omega^{\lambda\varphi}&=\partial\Omega^{\lambda u}\cap\partial\Omega^{\lambda T}=\partial\Omega,\\ \partial\Omega^{\lambda\omega}\cup\partial\Omega^{\lambda\varphi}&=\partial\Omega^{\lambda u}\cup\partial\Omega^{\lambda T}=0\end{aligned}\tag{3.6}$$

Utilizing the asymptotic expansion [82,83,84] of displacement and electric potential fields yields

$$u_i^\lambda(\mathbf{X})=u_i(\mathbf{X},\mathbf{Y})=u_i^0(\mathbf{X})+\lambda u_i^1(\mathbf{X},\mathbf{Y})+\lambda^2u_i^2(\mathbf{X},\mathbf{Y})+O(\lambda^3),\tag{3.7}$$

$$\varphi^\lambda(\mathbf{X})=\varphi(\mathbf{X},\mathbf{Y})=\varphi^0(\mathbf{X})+\lambda\varphi^1(\mathbf{X},\mathbf{Y})+\lambda^2\varphi^2(\mathbf{X},\mathbf{Y})+O(\lambda^3).\tag{3.8}$$

The size of the unit cell is of the order $\lambda$ and in the limit it is assumed to be infinitesimally small, so that first terms in asymptotic expansions for $u_i^\lambda(\mathbf{X})$ and $\varphi^0(\mathbf{X})$ do not depend on fine-scale coordinate **Y**. This has been shown to be a unique solution for linear elliptic problems. Note that for certain class of nonlinear problems, such as problems involving softening and localizations as well as neutronic diffusion, radiative transport problems [85], one has to consider large oscillations in the leading order term in which case the first term in asymptotic expansion will depend on fine-scale coordinates **Y.**

Expanding every term in (3.7) and (3.8) in Taylor series around the unit cell centroid $\mathbf{X}=\hat{\mathbf{X}}$ yields

$$u_i^0(\mathbf{X})=u_i^0(\hat{\mathbf{X}})+\lambda\left.\frac{\partial u_i^0}{\partial X_J}\right|_{\hat{\mathbf{X}}}Y_J+\lambda^2\left.\frac{\partial^2u_i^0}{\partial X_J\partial X_K}\right|_{\hat{\mathbf{X}}}Y_JY_K+O(\lambda^3),\tag{3.9}$$

$$u_i^n(\mathbf{X},\mathbf{Y})=u_i^n(\hat{\mathbf{X}},\mathbf{Y})+\lambda\left.\frac{\partial u_i^n}{\partial X_J}\right|_{\hat{\mathbf{X}}}Y_J+\lambda^2\left.\frac{\partial^2u_i^n}{\partial X_J\partial X_K}\right|_{\hat{\mathbf{X}}}Y_JY_K+O(\lambda^3),\tag{3.10}$$

$$\varphi^0(\mathbf{X})=\varphi^0(\hat{\mathbf{X}})+\lambda\left.\frac{\partial\varphi^0}{\partial X_J}\right|_{\hat{\mathbf{X}}}Y_J+\lambda^2\left.\frac{\partial^2\varphi^0}{\partial X_J\partial X_K}\right|_{\hat{\mathbf{X}}}Y_JY_K+O(\lambda^3),\tag{3.11}$$

$$\varphi^n(\mathbf{X},\mathbf{Y})=\varphi^n(\hat{\mathbf{X}},\mathbf{Y})+\lambda\left.\frac{\partial\varphi^n}{\partial X_J}\right|_{\hat{\mathbf{X}}}Y_J+\lambda^2\left.\frac{\partial^2\varphi^n}{\partial X_J\partial X_K}\right|_{\hat{\mathbf{X}}}Y_JY_K+O(\lambda^3),\tag{3.12}$$

where $X_J-\hat{X}_J=\lambda Y_J$ was used.

Substituting the above into asymptotic expansions (3.7), (3.8) gives the modified asymptotic expansion

$$u_i^\lambda(\mathbf{X})=u_i(\hat{\mathbf{X}},\mathbf{Y})=\hat{u}_i^0(\hat{\mathbf{X}})+\lambda\hat{u}_i^1(\hat{\mathbf{X}},\mathbf{Y})+\lambda^2\hat{u}_i^2(\hat{\mathbf{X}},\mathbf{Y})+O(\lambda^3),\tag{3.13}$$

where

$$\hat{u}_i^0\left(\hat{\mathbf{X}}\right)=u_i^0\left(\hat{\mathbf{X}}\right),\quad \hat{u}_i^1\left(\hat{\mathbf{X}},\mathbf{Y}\right)=u_i^1\left(\hat{\mathbf{X}},\mathbf{Y}\right)+\left.\frac{\partial u_i^0}{\partial X_J}\right|_{\hat{\mathbf{x}}} Y_J,$$
$$\hat{u}_i^2\left(\hat{\mathbf{X}},\mathbf{Y}\right)=u_i^2\left(\hat{\mathbf{X}},\mathbf{Y}\right)+\left.\frac{\partial u_i^1}{\partial X_J}\right|_{\hat{\mathbf{x}}} Y_J+\frac{1}{2}\left.\frac{\partial^2 u_i^0}{\partial X_J\partial X_K}\right|_{\hat{\mathbf{x}}} Y_J Y_k \tag{3.14}$$

and similarly for potential

$$\varphi^\lambda\left(\mathbf{X}\right)=\varphi\left(\hat{\mathbf{X}},\mathbf{Y}\right)=\hat{\varphi}^0\left(\hat{\mathbf{X}}\right)+\lambda\hat{\varphi}^1\left(\hat{\mathbf{X}},\mathbf{Y}\right)+\lambda^2\hat{\varphi}^2\left(\hat{\mathbf{X}},\mathbf{Y}\right)+O\left(\lambda^3\right), \tag{3.15}$$

where

$$\hat{\varphi}^0\left(\hat{\mathbf{X}}\right)=\varphi^0\left(\hat{\mathbf{X}}\right),\quad \hat{\varphi}^1\left(\hat{\mathbf{X}},\mathbf{Y}\right)=\varphi^1\left(\hat{\mathbf{X}},\mathbf{Y}\right)+\left.\frac{\partial\varphi^0}{\partial X_J}\right|Y_J,$$
$$\hat{\varphi}^2\left(\hat{\mathbf{X}},\mathbf{Y}\right)=\varphi^2\left(\hat{\mathbf{X}},\mathbf{Y}\right)+\left.\frac{\partial\varphi^1}{\partial X_J}\right|_{\hat{\mathbf{x}}} Y_J+\frac{1}{2}\left.\frac{\partial^2\varphi^0}{\partial X_J\partial X_k}\right|_{\hat{\mathbf{x}}} Y_J Y_K \tag{3.16}$$

In the classical homogenization the spatial derivative is defined as $\frac{\partial f^\lambda}{\partial X_I}=\frac{\partial f\left(\mathbf{X},\mathbf{Y}\right)}{\partial X_I}+\frac{1}{\xi}\frac{\partial f\left(\mathbf{X},\mathbf{Y}\right)}{\partial Y_I}$. Since in the modified asymptotic expansions (3.13) and (3.15) all terms are calculated with respect to the UC centroid $\hat{\mathbf{X}}$, there is no dependence on $\mathbf{X}$ and the spatial derivative reduces to

$$\frac{\partial f^\lambda\left(\mathbf{X}\right)}{\partial X_i}=\frac{1}{\lambda}\frac{\partial f\left(\hat{\mathbf{X}},\mathbf{Y}\right)}{\partial \mathbf{Y}_i}. \tag{3.17}$$

Thus displacement gradient may be expressed as

$$\frac{\partial u_i^\lambda}{\partial X_K}=\frac{1}{\lambda}\frac{\partial u_i\left(\hat{\mathbf{X}},\mathbf{Y}\right)}{\partial Y_K}=\frac{\partial\hat{u}_i^1\left(\hat{\mathbf{X}},\mathbf{Y}\right)}{\partial Y_K}+\lambda\frac{\partial\hat{u}_i^2\left(\hat{\mathbf{X}},\mathbf{Y}\right)}{\partial Y_K}+O\left(\lambda^2\right), \tag{3.18}$$

where

$$\frac{\partial\hat{u}_i^1\left(\hat{\mathbf{X}},\mathbf{Y}\right)}{\partial Y_K}=\frac{\partial u_i^1\left(\hat{\mathbf{X}},\mathbf{Y}\right)}{\partial Y_K}+\left.\frac{\partial u_i^0\left(\mathbf{X}\right)}{\partial X_K}\right|_{\hat{\mathbf{x}}},$$
$$\frac{\partial\hat{u}_i^2\left(\hat{\mathbf{X}},\mathbf{Y}\right)}{\partial Y_K}=\frac{\partial u_i^2\left(\hat{\mathbf{X}},\mathbf{Y}\right)}{\partial Y_K}+\left.\frac{\partial u_i^1\left(\mathbf{X},\mathbf{Y}\right)}{\partial X_K}\right|_{\hat{\mathbf{x}}}+\left.\frac{\partial^2 u_i^1\left(\mathbf{X},\mathbf{Y}\right)}{\partial X_J\partial Y_K}\right|_{\hat{\mathbf{x}}} Y_J+\left.\frac{\partial^2 u_i^0\left(\mathbf{X},\mathbf{Y}\right)}{\partial X_J\partial X_K}\right|_{\hat{\mathbf{x}}} Y_J. \tag{3.19}$$

The asymptotic expansion of the deformation gradient is given as

$$F_{iK}^\lambda=\delta_{iK}+\frac{\partial u_i^\lambda}{\partial X_K}=F_{iK}^0\left(\hat{\mathbf{X}},\mathbf{Y}\right)+\lambda F_{iK}^1\left(\hat{\mathbf{X}},\mathbf{Y}\right)+O\left(\lambda^2\right), \tag{3.20}$$

where

$$F_{iK}^{0}\left(\hat{\mathbf{X}},\mathbf{Y}\right)=\delta_{iK}+\frac{\partial\hat{u}_{i}^{1}\left(\hat{\mathbf{X}},\mathbf{Y}\right)}{\partial Y_{K}}=\delta_{iK}+\frac{\partial u_{i}^{1}\left(\hat{\mathbf{X}},\mathbf{Y}\right)}{\partial Y_{K}}+\left.\frac{\partial u_{i}^{0}\left(\mathbf{X}\right)}{\partial X_{K}}\right|_{\hat{\mathbf{X}}}=F_{iK}^{C}\left(\hat{\mathbf{X}},\mathbf{Y}\right)+F_{iK}^{*}\left(\hat{\mathbf{X}},\mathbf{Y}\right),\tag{3.21}$$

$$F_{iK}^{C}\left(\hat{\mathbf{X}}\right)=\delta_{iK}+\left.\frac{\partial u_{i}^{0}\left(\mathbf{X}\right)}{\partial X_{K}}\right|_{\hat{\mathbf{X}}}\equiv\left.\frac{\partial x_{i}}{\partial X_{K}}\right|_{\hat{\mathbf{X}}},\ F_{iK}^{*}\left(\hat{\mathbf{X}},\mathbf{Y}\right)=\frac{\partial u_{i}^{1}\left(\hat{\mathbf{X}},\mathbf{Y}\right)}{\partial Y_{K}},\ F_{iK}^{1}\left(\hat{\mathbf{X}},\mathbf{Y}\right)=\frac{\partial\hat{u}_{i}^{2}\left(\hat{\mathbf{X}},\mathbf{Y}\right)}{\partial Y_{k}}.\tag{3.22}$$

Similarly, the electric field is given as negative derivatives of electric potential

$$\begin{aligned}&\mathcal{E}_{J}^{\lambda}\left(\mathbf{X}\right)=-\frac{\partial\varphi^{\lambda}}{\partial X_{J}}=-\frac{1}{\lambda}\frac{\partial\varphi\left(\hat{\mathbf{X}},\mathbf{Y}\right)}{\partial Y_{J}}=-\frac{\partial\hat{\varphi}^{1}\left(\hat{\mathbf{X}},\mathbf{Y}\right)}{\partial Y_{J}}-\lambda\frac{\partial\hat{\varphi}^{2}\left(\hat{\mathbf{X}},\mathbf{Y}\right)}{\partial Y_{J}}+O\left(\lambda^{2}\right)=\\&=\mathcal{E}_{J}^{0}\left(\hat{\mathbf{X}},\mathbf{Y}\right)+\lambda\mathcal{E}_{J}^{1}\left(\hat{\mathbf{X}},\mathbf{Y}\right)+O\left(\lambda^{2}\right),\end{aligned}\tag{3.23}$$

where

$$\mathcal{E}_{J}^{0}\left(\hat{\mathbf{X}},\mathbf{Y}\right)=-\frac{\partial\hat{\varphi}^{1}}{\partial Y_{J}}=-\frac{\partial\varphi^{1}\left(\hat{\mathbf{X}},\mathbf{Y}\right)}{\partial Y_{J}}-\left.\frac{\partial\varphi^{0}\left(\mathbf{X}\right)}{\partial X_{J}}\right|_{\hat{\mathbf{X}}}=\mathcal{E}_{J}^{C}\left(\hat{\mathbf{X}}\right)+\mathcal{E}_{J}^{*}\left(\hat{\mathbf{X}},\mathbf{Y}\right),\tag{3.24}$$

$$\mathcal{E}_{J}^{C}\left(\hat{\mathbf{X}}\right)=-\left.\frac{\partial\varphi^{0}\left(\mathbf{X}\right)}{\partial X_{J}}\right|_{\hat{\mathbf{X}}},\ \mathcal{E}_{J}^{*}\left(\hat{\mathbf{X}},\mathbf{Y}\right)=-\frac{\partial\varphi^{1}\left(\hat{\mathbf{X}},\mathbf{Y}\right)}{\partial Y_{J}},\ \mathcal{E}_{J}^{1}\left(\hat{\mathbf{X}},\mathbf{Y}\right)=-\frac{\partial\hat{\varphi}^{2}}{\partial Y_{J}}.\tag{3.25}$$

The coarse-scale deformation gradient $F_{iK}^{C}$ and electric field $\mathcal{E}_{J}^{C}$ are related to the average of the leading order deformation gradient $F_{iK}^{0}\left(\hat{\mathbf{X}},\mathbf{Y}\right)$ in (3.21) and electric field $\mathcal{E}_{J}^{0}\left(\hat{\mathbf{X}},\mathbf{Y}\right)$ in (3.24) over the unit cell domain

$$F_{iK}^{C}\left(\hat{\mathbf{X}}\right)=\frac{1}{\Theta_{Y}}\int_{\Theta_{Y}}F_{iK}^{0}\left(\hat{\mathbf{X}},\mathbf{Y}\right)d\Theta_{Y}=\delta_{iK}+\left.\frac{\partial u_{i}^{0}\left(\mathbf{X}\right)}{\partial X_{K}}\right|_{\hat{X}},\tag{3.26}$$

$$\mathcal{E}_{J}^{C}\left(\hat{\mathbf{X}}\right)=\frac{1}{\left|\Theta_{Y}\right|}\int_{\Theta_{Y}}\mathcal{E}_{J}^{0}\left(\hat{\mathbf{X}},\mathbf{Y}\right)d\Theta=-\left.\frac{\partial\varphi^{0}}{\partial X_{J}}\right|_{\hat{\mathbf{X}}},\tag{3.27}$$

where conditions $\int_{\Theta_{Y}}\frac{\partial u_{i}^{1}}{\partial Y_{J}}d\Theta=0$ and $\int_{\Theta_{Y}}\frac{\partial\varphi^{1}}{\partial Y_{J}}d\Theta=0$ were employed. These conditions correspond to periodicity (or weak periodicity) of fine-scale displacement and potential fields, which will be discussed in the next section.

Expanding stress and electric displacement in Taylor series around the leading order deformation gradient $\mathbf{F}^{0}\left(\mathbf{X},\mathbf{Y}\right)$ and electric field $\boldsymbol{\mathcal{E}}^{0}\left(\hat{\mathbf{X}},\mathbf{Y}\right)$ yields

$$K_{iJ}^{\lambda}\left(\mathbf{F}^{\lambda},\boldsymbol{\mathcal{E}}^{\lambda}\right)=K_{iJ}\left(\mathbf{F}^{0},\boldsymbol{\mathcal{E}}^{0}\right)+\lambda\left.\frac{\partial K_{iJ}}{\partial F_{mN}}\right|_{\mathbf{F}^{0},\mathbf{E}^{0}}F_{mN}^{1}+\lambda\left.\frac{\partial K_{iJ}}{\partial \mathcal{E}_{M}}\right|_{\mathbf{F}^{0},\mathbf{E}^{0}}\mathcal{E}_{M}^{1}+O\left(\lambda^{2}\right)=K_{iJ}^{0}+\lambda K_{iJ}^{1}+O\left(\lambda^{2}\right) \tag{3.28}$$

$$\mathcal{D}_{J}^{\lambda}\left(\mathbf{F}^{\lambda},\boldsymbol{\mathcal{E}}^{\lambda}\right)=\mathcal{D}_{J}\left(\mathbf{F}^{0},\boldsymbol{\mathcal{E}}^{0}\right)+\lambda\left.\frac{\partial \mathcal{D}_{J}}{\partial F_{mN}}\right|_{\mathbf{F}^{0},\mathbf{E}^{0}}F_{mN}^{1}+\lambda\left.\frac{\partial \mathcal{D}_{J}}{\partial \mathcal{E}_{M}}\right|_{\mathbf{F}^{0},\mathbf{E}^{0}}\mathcal{E}_{M}^{1}+O\left(\lambda^{2}\right)=\mathcal{D}_{J}^{0}+\lambda\mathcal{D}_{J}^{1}+O\left(\lambda^{2}\right) \tag{3.29}$$

Taylor expansion of stress and electric displacement around the unit cell centroid $\hat{\mathbf{X}}$ yields

$$K_{iJ}\left(\mathbf{F}^{\lambda},\boldsymbol{\mathcal{E}}^{\lambda}\right)=K_{iJ}\left(\mathbf{X},\mathbf{Y}\right)=K_{iJ}^{0}\left(\hat{\mathbf{X}},\mathbf{Y}\right)+\lambda\left(\left.\frac{\partial K_{iJ}^{0}}{\partial X_{K}}\right|_{\hat{\mathbf{X}}}Y_{K}+K_{iJ}^{1}\left(\hat{\mathbf{X}},\mathbf{Y}\right)\right)+O\left(\lambda^{2}\right), \tag{3.30}$$

$$\mathcal{D}_{J}\left(\mathbf{F}^{\lambda},\boldsymbol{\mathcal{E}}^{\lambda}\right)=\mathcal{D}_{J}\left(\hat{\mathbf{X}},\mathbf{Y}\right)=\mathcal{D}_{J}^{0}\left(\hat{\mathbf{X}},\mathbf{Y}\right)+\lambda\left(\left.\frac{\partial \mathcal{D}_{J}^{0}}{\partial X_{K}}\right|_{\hat{X}}Y_{K}+\mathcal{D}_{J}^{1}\left(\hat{\mathbf{X}},\mathbf{Y}\right)\right)+O\left(\lambda^{2}\right). \tag{3.31}$$

Again, here the relation $\left(X_{i}-\hat{X}_{i}\right)=\lambda Y_{i}$ has been utilized. Further substituting above into equilibrium equation (3.3) and Gauss law (3.4) yields

$$\lambda^{-1}\frac{\partial K_{iJ}^{0}\left(\hat{\mathbf{X}},\mathbf{Y}\right)}{\partial Y_{J}}+\left.\frac{\partial K_{iJ}^{0}}{\partial X_{J}}\right|_{\hat{X}}+\frac{\partial K_{iJ}^{1}\left(\hat{\mathbf{X}},\mathbf{Y}\right)}{\partial Y_{J}}+B_{i}\left(\hat{\mathbf{X}},\mathbf{Y}\right)-\rho_{M}\left(\hat{\mathbf{X}},\mathbf{Y}\right)\frac{\partial^{2}\hat{u}_{i}^{0}\left(\hat{\mathbf{X}},t\right)}{\partial t^{2}}=0, \tag{3.32}$$

$$\lambda^{-1}\frac{\partial \mathcal{D}_{J}^{0}\left(\hat{\mathbf{X}},\mathbf{Y}\right)}{\partial Y_{J}}+\left.\frac{\partial \mathcal{D}_{J}^{0}}{\partial X_{J}}\right|_{\hat{X}}+\frac{\partial \mathcal{D}_{J}^{1}\left(\hat{\mathbf{X}},\mathbf{Y}\right)}{\partial Y_{J}}-\rho_{E}\left(\hat{\mathbf{X}},\mathbf{Y}\right)=0. \tag{3.33}$$

Collecting terms of equal orders in (3.32), (3.33) yields the two-scale equilibrium equation and Gauss law

$$O\left(\lambda^{-1}\right):\ \frac{\partial K_{iJ}^{0}\left(\hat{\mathbf{X}},\mathbf{Y}\right)}{\partial Y_{J}}=0,\quad \frac{\partial \mathcal{D}_{J}^{0}\left(\hat{\mathbf{X}},\mathbf{Y}\right)}{\partial Y_{J}}=0, \tag{3.34}$$

$$\begin{aligned}O\left(\lambda^{0}\right):\ &\frac{\partial K_{iJ}^{0}}{\partial X_{J}}+\frac{\partial K_{iJ}^{1}\left(\hat{\mathbf{X}},\mathbf{Y}\right)}{\partial Y_{J}}+B_{i}\left(\hat{\mathbf{X}},\mathbf{Y}\right)=\rho_{M}\left(\hat{\mathbf{X}},\mathbf{Y}\right)\frac{\partial^{2}\hat{u}_{i}^{0}\left(\hat{\mathbf{X}},t\right)}{\partial t^{2}},\\ &\frac{\partial \mathcal{D}_{J}^{0}}{\partial X_{J}}+\frac{\partial \mathcal{D}_{J}^{1}\left(\hat{\mathbf{X}},\mathbf{Y}\right)}{\partial Y_{J}}=\rho_{E}\left(\hat{\mathbf{X}},\mathbf{Y}\right).\end{aligned} \tag{3.35}$$

Integrating $O\left(\lambda^0\right)$ equations over the unit cell domain and exploiting $\int_\Theta \frac{\partial K_{iJ}^1\left(\hat{\mathbf{X}},\mathbf{Y}\right)}{\partial Y_J} dY = 0$, $\int_\Theta \frac{\partial \mathcal{D}_J^1\left(\hat{\mathbf{X}},\mathbf{Y}\right)}{\partial Y_J} dY = 0$, which correspond to periodicity (or weak periodicity) of fine-scale stress and electric displacement, yields the coarse-scale equations

$$\begin{aligned} &\left.\frac{\partial K_{iJ}^C\left(\mathbf{X}\right)}{\partial X_J}\right|_{\hat{\mathbf{X}}} + B^C{}_i\left(\hat{\mathbf{X}}\right) = \bar{\rho}_M\left(\hat{\mathbf{X}}\right)\frac{\partial^2 \hat{u}_i^0\left(\hat{\mathbf{X}},t\right)}{\partial t^2}, \\ &\left.\frac{\partial \mathcal{D}_J^C\left(\mathbf{X}\right)}{\partial X_J}\right|_{\hat{\mathbf{X}}} = \rho_E^C\left(\hat{\mathbf{X}}\right), \end{aligned} \tag{3.36}$$

where

$$K_{iJ}^C\left(\hat{\mathbf{X}}\right) = \frac{1}{\Theta_Y}\int_{\Theta_Y} K_{iJ}^0\left(\mathbf{F}^0\left(\hat{\mathbf{X}},\mathbf{Y}\right),\boldsymbol{\mathcal{E}}\left(\hat{\mathbf{X}},\mathbf{Y}\right)\right)d\Theta,\ \ B_i^C\left(\hat{\mathbf{X}}\right) = \frac{1}{\Theta_Y}\int_{\Theta_Y} B_i\left(\hat{\mathbf{X}},\mathbf{Y}\right)d\Theta, \tag{3.37}$$

$$\mathcal{D}_J^C\left(\hat{\mathbf{X}}\right) = \frac{1}{\Theta_Y}\int_{\Theta_Y} \mathcal{D}_J^0\left(\mathbf{F}^0\left(\hat{\mathbf{X}},\mathbf{Y}\right),\boldsymbol{\mathcal{E}}\left(\hat{\mathbf{X}},\mathbf{Y}\right)\right)d\Theta,\ \ \rho_E^C\left(\mathbf{X}\right) = \frac{1}{\Theta_Y}\int_{\Theta_Y} \rho_E\left(\hat{\mathbf{X}},\mathbf{Y}\right)d\Theta. \tag{3.38}$$

Hereafter we will make use of an argument of the unit cell infinitesimality by which the unit cell centroid $\hat{\mathbf{X}}$ can be positioned at an arbitrary point $\mathbf{X}$. Therefore, the centroid $\hat{\mathbf{X}}$ can be replaced by an arbitrary point $\mathbf{X}$. Equations (3.36) with boundary conditions (3.5) define the coarse-scale boundary value problem.

The set of equations (3.34) together with periodic (or weakly periodic) boundary conditions, discussed in the next section, defines fine-scale boundary value problem.

## 4. Boundary conditions for the unit cell problem

In this section various boundary conditions imposed on the unit cell will be considered. The most common are the periodic boundary conditions, when the displacement and electric potential perturbations on the opposite sides of the unit cell are assumed to be equal.

Consider the asymptotic expansions for displacement and electric potential fields (3.13), (3.15)

$$u_i^\lambda\left(\mathbf{X},t\right) = u_i\left(\hat{\mathbf{X}},\mathbf{Y},t\right) = u_i^0\left(\hat{\mathbf{X}},t\right) + \lambda\left[\left(F_{iJ}^C\left(\hat{\mathbf{X}},t\right) - \delta_{iJ}\right)Y_J + u_i^1\left(\hat{\mathbf{X}},\mathbf{Y},t\right)\right] + O\left(\lambda^2\right),$$

$$\varphi^\lambda\left(\mathbf{X},t\right) = \varphi\left(\hat{\mathbf{X}},\mathbf{Y},t\right) = \varphi^0\left(\hat{\mathbf{X}},t\right) + \lambda\left[-\mathcal{E}_J^C\left(\hat{\mathbf{X}},t\right)Y_J + \varphi^1\left(\hat{\mathbf{X}},\mathbf{Y},t\right)\right] + O\left(\lambda^2\right),$$

where (3.25) and (3.26) were used. The leading order terms, which represent the rigid body translation of the unit cell and constant potential, are independent of the unit cell coordinates **Y**. The $O(\lambda)$ terms describe the unit cell distortion and electric field in it. The terms $\left(F_{iJ}^{C}\left(\hat{\mathbf{X}},t\right)-\delta_{iJ}\right)Y_J$ and $\mathcal{E}_J^C\left(\hat{\mathbf{X}},t\right)Y_J$ represent a uniform coarse-scale deformation and uniform coarse-scale electric field, while the terms $u_i^1\left(\hat{\mathbf{X}},\mathbf{Y},t\right)$ and $\varphi^1\left(\hat{\mathbf{X}},\mathbf{Y},t\right)$ capture *the deviations from the uniform fields induced by material heterogeneity*. These terms are important for electrostriction effect [26]. Making these terms larger increases the electrostriction effect.

Figures 4(a) and 4(b) show the initial and deformed shape of the unit cell, respectively. The dotted line in Figure 3(b) depicts the deformed shape of the unit cell due to $\left(F_{iJ}^{C}\left(\hat{\mathbf{X}},t\right)-\delta_{iJ}\right)Y_J$, whereas the solid line shows the contribution of the two $O(\lambda)$ terms.

At the unit cell vertices $\partial\Theta_Y^{vert}$, the deviations from the uniform fields, $u_i^1\left(\hat{\mathbf{X}},\mathbf{Y},t\right)$ and $\varphi^1\left(\hat{\mathbf{X}},\mathbf{Y},t\right)$, are assumed to vanish. For the remaining points on the boundary of the unit cell, the deviations from the average $u_i^1\left(\hat{\mathbf{X}},\mathbf{Y},t\right)$, $\varphi_i^1\left(\hat{\mathbf{X}},\mathbf{Y},t\right)$ are prescribed to be periodic functions. Figure 4 depicts two points M and S on the opposite faces of the unit cell with M and S termed as the master and slave points, respectively. The displacements of the two points are given as

$$\hat{u}_i^1\left(\hat{\mathbf{X}},\mathbf{Y}^M,t\right)=\left(F_{iJ}^{C}\left(\hat{\mathbf{X}},t\right)-\delta_{iJ}\right)Y_J^M+u_i^1\left(\hat{\mathbf{X}},\mathbf{Y}^M,t\right), \tag{4.1}$$

$$\hat{u}_i^1\left(\hat{\mathbf{X}},\mathbf{Y}^S,t\right)=\left(F_{iJ}^{C}\left(\hat{\mathbf{X}},t\right)-\delta_{iJ}\right)Y_J^S+u_i^1\left(\hat{\mathbf{X}},\mathbf{Y}^S,t\right). \tag{4.2}$$

Subtracting equation (4.2) from (4.1) and accounting for periodicity, i.e. $u_i^1\left(\hat{\mathbf{X}},\mathbf{Y}^M,t\right)=u_i^1\left(\hat{\mathbf{X}},\mathbf{Y}^S,t\right)$, gives a multi-point constraint (MPC) equation

$$\hat{u}_i^1\left(\hat{\mathbf{X}},\mathbf{Y}^M,t\right)-\hat{u}_i^1\left(\hat{\mathbf{X}},\mathbf{Y}^S,t\right)=\left(F_{iJ}^{C}\left(\hat{\mathbf{X}},t\right)-\delta_{iJ}\right)\left(Y_J^M-Y_J^S\right) \tag{4.3}$$

where $\boldsymbol{Y}^{\mathrm{M}}$ and $\boldsymbol{Y}^{\mathrm{S}}$ represent the local coordinates of the master and slave nodes on the unit cell boundary, respectively.

Similarly, periodicity of electric potential perturbations $\varphi^1\left(\hat{\mathbf{X}},\mathbf{Y}^M,t\right)=\varphi^1\left(\hat{\mathbf{X}},\mathbf{Y}^S,t\right)$ gives the following constraint equation

$$\hat{\varphi}\left(\hat{\mathbf{X}},\mathbf{Y}^M,t\right)-\hat{\varphi}\left(\hat{\mathbf{X}},\mathbf{Y}^S,t\right)=-\mathcal{E}_J^C\left(\hat{\mathbf{X}},t\right)\left(Y_J^M-Y_J^S\right). \tag{4.4}$$

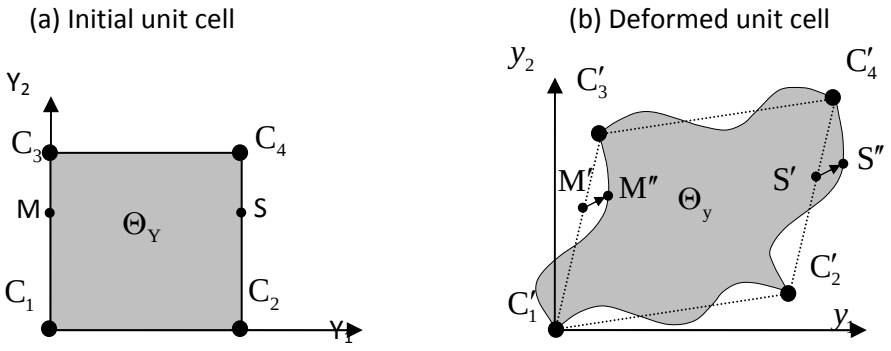


Figure 4: Definition of periodic boundary conditions

Periodic boundary conditions can be used for periodic heterogeneous medium and when the unit cell distortion is not considerable, otherwise they are not physical. For nonperiodic medium or in case of large unit cell distortions more general boundary conditions have to be used instead. Note that the only time when the periodicity condition was exercised was in deriving equations (3.26), (3.27). For (3.26), (3.27) to hold the following conditions must be satisfied

$$\int_{\Theta_Y} \frac{\partial u_i^1(\boldsymbol{X},\boldsymbol{Y},t)}{\partial Y_J} d\Theta_Y = 0, \ \int_{\Theta_Y} \frac{\partial \varphi^1(\boldsymbol{X},\boldsymbol{Y},t)}{\partial Y_J} d\Theta_Y = 0. \tag{4.5}$$

Applying Green's theorem and exploiting relations (3.14)b, (3.16)b, and (3.26), (3.27) the above reduces to

$$\begin{aligned} &\int_{\partial\Theta_Y} \left( \hat{u}_i^1\left(\hat{\mathbf{X}},\mathbf{Y},t\right) - \left( F_{iK}^C\left(\hat{\mathbf{X}},t\right) - \delta_{iK} \right) Y_K \right) N_K d\Gamma_Y = 0, \\ &\int_{\partial\Theta_Y} \left( \hat{\varphi}^1\left(\hat{\mathbf{X}},\mathbf{Y},t\right) - \left( -E_K^C\left(\hat{\mathbf{X}},t\right) \right) Y_K \right) N_K d\Gamma_Y = 0, \end{aligned} \tag{4.6}$$

where $\partial\Theta_Y$ is the boundary of $\Theta_Y$ and $N_K$ are the components of the unit normal to the boundary $\partial\Theta_Y$. Equation (4.6) represents the so-called *weak periodicity* condition.

Alternatively to equations (4.3), (4.4) and (4.6) an essential boundary condition

$$\begin{aligned} &\hat{u}_i^1\left(\hat{\mathbf{X}},\mathbf{Y},t\right) - \left( F_{iK}^C\left(\hat{\mathbf{X}},t\right) - \delta_{iK} \right) Y_K = 0, \\ &\hat{\varphi}^1\left(\hat{\mathbf{X}},\mathbf{Y},t\right) - \left( -E_K^C\left(\hat{\mathbf{X}},t\right) \right) Y_K = 0 \end{aligned} \tag{4.7}$$

is often exercised in practice. It corresponds to zero perturbations from coarse-scale fields on the unit cell boundary.

The essential boundary conditions can be enforced either in the strong form (4.7) or in the weak form as

$$\begin{aligned}
&\int_{\partial\Theta_Y} \left( \hat{u}_i^1\left(\hat{\mathbf{X}},\mathbf{Y},t\right) - \left( F_{iK}^C\left(\hat{\mathbf{X}},t\right) - \delta_{iK} \right) Y_K \right) \mu_i d\Gamma_Y = 0, \\
&\int_{\partial\Theta_Y} \left( \hat{\varphi}^1\left(\hat{\mathbf{X}},\mathbf{Y},t\right) - \left( -E_K^C\left(\hat{\mathbf{X}},t\right) \right) Y_K \right) \mu_\varphi d\Gamma_Y = 0
\end{aligned} \tag{4.8}$$

where $\mu_i, \mu_\varphi$ are the Lagrange multipliers representing unknown tractions and surface charge density on $\partial\Theta_Y$. If we choose $\mu_i = K_{iJ}^C N_J$, $\mu_\varphi = \mathcal{D}_J^C N_J$ where $K_{iJ}^C, \mathcal{D}_J^C$ are constant over $\Theta_Y$ and require (4.8) to be satisfied for arbitrary $K_{iJ}^C$ and $\mathcal{D}_J^C$, we then obtain equation (4.6). Therefore, equation (4.6) will be referred to as a weak compatibility boundary condition while equation (4.7) as the strong compatibility condition. Equation (4.6) is in the spirit of the work of Mesarovic [86] who imposed the unit cell to satisfy average small strains.

The different boundary conditions can be denoted for generality

$$\boldsymbol{g}\left( \begin{bmatrix} \hat{\boldsymbol{u}}^1 \\ \varphi^1 \end{bmatrix} \right) = 0 \quad on \quad \partial\Theta_Y \tag{4.9}$$

## 5. Two-scale problem

The two-scale problem, consisting of the unit cell equations (3.34) subjected to periodic (or other) boundary conditions (4.9) and the coarse-scale equations (3.36), is two-way coupled. The link between the two scales is schematically shown in Figure 5.

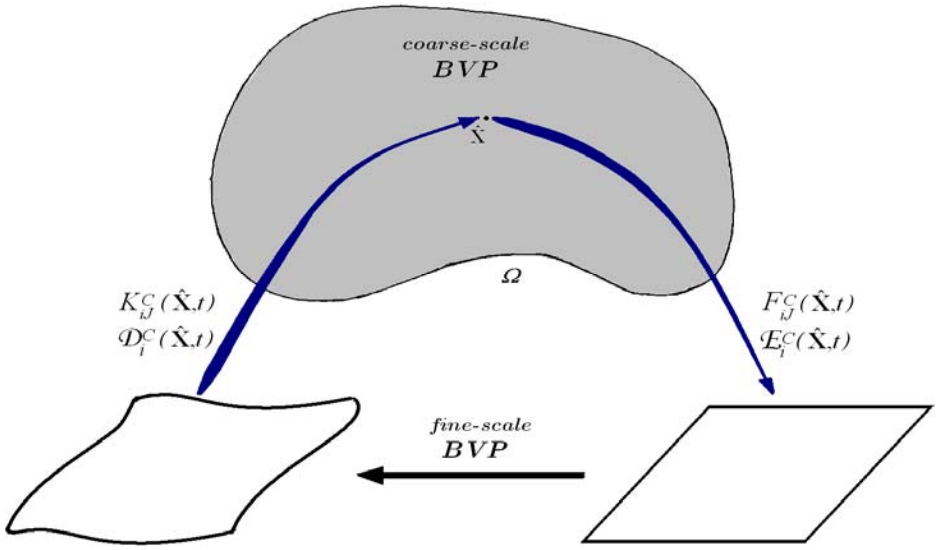


Figure 5: Information transfer between the coarse-scale and fine-scale problems

The fine-scale problem is driven by the overall (coarse-scale) deformation gradient $F_{iK}^C\left(\hat{\mathbf{X}},t\right)$ and electric field $\mathcal{E}_K^C\left(\hat{\mathbf{X}},t\right)$. They are calculated for every material point of the coarse-scale problem (in practice only for integration points of the coarse mesh) and used together with (4.9) to formulate boundary conditions to be imposed on the unit cell. Once the unit cell problem is solved, it provides the coarse-scale problem with coarse-scale stress $K_{iJ}^C$ and electric displacement $\mathcal{D}_J^C$ via (3.37), (3.38).

This effectively provides a coarse-scale constitutive relationship. Additionally, the local coarse-scale consistent tangent is derived from the fine-scale stiffness.

This scale-bridging approach belongs to the category of *information-passing* (sometimes referred to as hierarchical or sequential) multiscale methods which evolve a coarse-scale model by advancing a sequence of fine-scale models in small windows (representative volume or unit cell) placed at the Gauss points of the discretized coarse-scale model.

The coupled two-scale problem is summarized below:

(a) Fine scale problem

$$
\begin{aligned}
&\textit{Given } F^C_{iK}(\hat{\boldsymbol{X}},t), \mathcal{E}^C_K(\hat{\boldsymbol{X}},t) \textit{ find } \hat{u}^1_i(\hat{\boldsymbol{X}},\boldsymbol{Y},t), \hat{\varphi}^1(\hat{\boldsymbol{X}},\boldsymbol{Y},t) \textit{ on } \Theta_Y \textit{ such that}: \\
&\frac{\partial K^C_{iJ}\left(\boldsymbol{F}\left(\hat{\boldsymbol{X}},\boldsymbol{Y},t\right),\boldsymbol{\mathcal{E}}\left(\hat{\boldsymbol{X}},\boldsymbol{Y},t\right)\right)}{\partial Y_J} = 0, \; \frac{\partial \mathcal{D}^C_J\left(\boldsymbol{F}\left(\hat{\boldsymbol{X}},\boldsymbol{Y},t\right),\boldsymbol{\mathcal{E}}\left(\hat{\boldsymbol{X}},\boldsymbol{Y},t\right)\right)}{\partial Y_J} = 0 \qquad \textit{on } \Theta_Y \\
&\boldsymbol{g}\left(\begin{bmatrix}\hat{\boldsymbol{u}}^1 \\ \hat{\varphi}^1\end{bmatrix}\right) = 0 \qquad \textit{on } \partial\Theta_Y
\end{aligned}
\tag{5.1}
$$

(b) Coarse-scale problem

$$
\begin{aligned}
&\textit{Given } K^C_{iJ},\ \mathcal{D}^C_J, \textit{ find } \hat{u}^0_i(\hat{\boldsymbol{X}},t), \hat{\varphi}^0(\hat{\boldsymbol{X}},t) \textit{ on } \Omega \textit{ such that} \\
&\frac{\partial K^C_{iJ}}{\partial X_J} + B^C_i = \overline{\rho}_X \frac{\partial^2 \hat{u}^0_i}{\partial t^2} \qquad \textit{on } \Omega \\
&\frac{\partial \mathcal{D}^C_J}{\partial X_J} - \overline{\rho}_e = 0 \\
&K^C_{iJ} N_J = \overline{T}_i \quad \textit{on } \partial\Omega^T; \;\; \hat{u}^0_i = \overline{u}_i \quad \textit{on } \partial\Omega^u \\
&\mathcal{D}^C_J N_J = \overline{\omega} \textit{ on } \partial\Omega^\omega; \;\; \hat{\varphi}^0 = \overline{\varphi} \;\; \textit{on} \;\; \partial\Omega^\varphi \\
&\hat{u}^0_i = \overline{u}^0_i \qquad \textit{at } t = 0; \quad \frac{\partial \hat{u}^0_i}{\partial t} = \overline{v}^0_i \quad \textit{at } t = 0
\end{aligned}
\tag{5.2}
$$

## 6. Finite element discretization

Both the coarse- and fine-scale problems are discretized using finite elements. The displacement and electric potential fields of the fine-scale problem $\hat{u}^1_i\left(\hat{\mathbf{X}},\mathbf{Y},t\right)$, $\hat{\varphi}^1\left(\hat{\mathbf{X}},\mathbf{Y},t\right)$ are approximated as

$$
\begin{aligned}
\hat{u}^1_i\left(\hat{\mathbf{X}},\mathbf{Y},t\right) &= N^1_B\left(\mathbf{Y}\right) d^1_{iB}\left(\hat{\mathbf{X}},t\right), \\
\hat{\varphi}^1\left(\hat{\mathbf{X}},\mathbf{Y},t\right) &= N^1_B\left(\mathbf{Y}\right) \varphi^1_B\left(\hat{\mathbf{X}},t\right),
\end{aligned}
\tag{6.1}
$$

where subscript $B$ denotes the node number, $N^1_B(\boldsymbol{Y})$ are the unit cell shape functions and $d^1_{iB}$, $\varphi^1_B$ are the nodal displacements and potentials in the unit cell mesh. Let $d^M_{iC}\left(\hat{\mathbf{X}},t\right)$, $\varphi^M_C\left(\hat{\mathbf{X}},t\right)$ be the

master (independent) degrees of freedom and express $d^1_{iB}$, $\varphi^1_B$ by a linear combination of $d^M_{jC}\left(\hat{\mathbf{X}},t\right)$ and $\varphi^M_C\left(\hat{\mathbf{X}},t\right)$ defined by

$$\begin{bmatrix} d^1_{iB}(\hat{\boldsymbol{X}},t) \\ \varphi^1_B(\hat{\boldsymbol{X}},t) \end{bmatrix} = \begin{bmatrix} T^d_{iBkC}(\hat{\boldsymbol{X}},t) & 0 \\ 0 & T^{\varphi}_{BC}(\hat{\boldsymbol{X}},t) \end{bmatrix} \begin{bmatrix} d^M_{kC}(\hat{\boldsymbol{X}},t) \\ \varphi^M_C(\hat{\boldsymbol{X}},t) \end{bmatrix} \tag{6.2}$$

so that the constraint equation (4.9) in the discrete form is satisfied

$$\boldsymbol{g}\left( N^1_B(\boldsymbol{Y}) \begin{bmatrix} T^d_{iBkC}(\hat{\boldsymbol{X}},t) & 0 \\ 0 & T^{\varphi}_{BC}(\hat{\boldsymbol{X}},t) \end{bmatrix} \begin{bmatrix} d^M_{kC}(\hat{\boldsymbol{X}},t) \\ \varphi^M_C(\hat{\boldsymbol{X}},t) \end{bmatrix} \right) = 0 \quad on \quad \partial\Theta_Y \tag{6.3}$$

Then writing the Galerkin weak form of (5.1) and discretizing it using (6.1) yields the discrete residual equation:

$$\begin{bmatrix} r^{d1}_{kC}({}^{m+1}_{n+1}\Delta\boldsymbol{d^1}, {}^{m+1}_{n+1}\Delta\varphi^1) \\ r^{\varphi 1}_{C}({}^{m+1}_{n+1}\Delta\boldsymbol{d^1}, {}^{m+1}_{n+1}\Delta\varphi^1) \end{bmatrix} \equiv \int_{\Theta_Y} \begin{bmatrix} T^d_{iBkC}(\hat{\boldsymbol{X}},t) & 0 \\ 0 & T^{\varphi}_{BC}(\hat{\boldsymbol{X}},t) \end{bmatrix} \frac{\partial N^1_B}{\partial Y_j}{}^{m+1}_{n+1} \begin{bmatrix} K_{iJ} \\ \mathcal{D}_J \end{bmatrix} d\Theta_Y = 0 \tag{6.4}$$

where the left subscript and superscript denote the load increment and the iteration count (for implicit method) at the coarse-scale, respectively; ${}^{m+1}_{n+1}r^{d1}_{iB}$ and $r^{\varphi 1}_C$, ${}^{m+1}_{n+1}\Delta d^1_{iB}$ and ${}^{m+1}_{n+1}\Delta\varphi^1$ are the residuals, displacement and potential increments in the $(m+1)^{\text{th}}$ iteration of the $(n+1)^{\text{th}}$ load increment, respectively. If the constitutive equations are defined in terms of the Cauchy stress and electric displacement in the current configuration it is convenient to restate the unit cell problem as follows:

Given ${}^{m+1}_{n+1}F^C_{iJ}, {}^{m+1}_{n+1}E^C_i$ and ${}_n\sigma_{ij}, {}_nD_i$ find ${}^{m+1}_{n+1}\Delta d^1_{iB}, {}^{m+1}_{n+1}\Delta\varphi^1_B$ such that:

$$\begin{bmatrix} r^{d1}_{kC}({}^{m+1}_{n+1}\Delta\boldsymbol{d^1}, {}^{m+1}_{n+1}\Delta\varphi^1) \\ r^{\varphi 1}_{C}({}^{m+1}_{n+1}\Delta\boldsymbol{d^1}, {}^{m+1}_{n+1}\Delta\varphi^1) \end{bmatrix} = \int_{\Theta_Y} \begin{bmatrix} T^d_{iBkC}(\hat{\boldsymbol{X}},t) & 0 \\ 0 & T^{\varphi}_{BC}(\hat{\boldsymbol{X}},t) \end{bmatrix} \frac{\partial N^1_B}{\partial Y_J}{}^{m+1}_{n+1} \begin{bmatrix} K_{iJ} \\ \mathcal{D}_J \end{bmatrix} d\Theta_Y = 0 \tag{6.5}$$

$$\begin{bmatrix} d^1_{iB}(\hat{\boldsymbol{X}},t) \\ \varphi^1_B(\hat{\boldsymbol{X}},t) \end{bmatrix} = \begin{bmatrix} T^d_{iBkC}(\hat{\boldsymbol{X}},t) & 0 \\ 0 & T^{\varphi}_{BC}(\hat{\boldsymbol{X}},t) \end{bmatrix} \begin{bmatrix} d^M_{kC}(\hat{\boldsymbol{X}},t) \\ \varphi^M_C(\hat{\boldsymbol{X}},t) \end{bmatrix}$$

where we have exploited the relation between the first Piola-Kirchhoff stress $K_{iK}$, electric displacement $\mathcal{D}_K$ in the Lagrangian description and their current configuration counterparts, Cauchy stress $\sigma_{ij}$ and electric displacement $D_i$

$$
\begin{aligned}
J\sigma_{ij} &= F_{jK}K_{iK}, \\
JD_i &= F_{iK}\mathcal{D}_K
\end{aligned}
\tag{6.6}
$$

and $J$ in (6.6) is the determinant of $F_{jK}$.

Similarly, the coarse-scale displacements and potential $\hat{u}_i^0(\hat{\boldsymbol{X}},t)$, $\hat{\varphi}^0(\hat{\boldsymbol{X}},t)$ are discretized as

$$
\begin{aligned}
\hat{u}_i^0(\hat{\boldsymbol{X}},t) &= N_A^C(\hat{\boldsymbol{X}})d_{iA}^C(t), \\
\hat{\varphi}^0(\hat{\boldsymbol{X}},t) &= N_A^C(\hat{\boldsymbol{X}})\varphi_A^C(t),
\end{aligned}
\tag{6.7}
$$

where $N_A^C(\hat{\boldsymbol{X}})$, $d_{iA}^C$ and $\varphi_A^C$ are the coarse-scale shape functions, nodal displacements and potential, respectively. Writing the weak form of (5.2) and using discretization (6.7) the discrete coarse-scale equations can be expressed as

Given ${}_{n+1}B_i^C, {}_{n+1}\rho_e^C,$ ${}_{n+1}\overline{T}_i$ and ${}_{n+1}\overline{\omega}$, find ${}_{n+1}\Delta d_{iA}^0$ and ${}_{n+1}\Delta\varphi_A^0$ such that:

$$
\begin{aligned}
&{}_{n+1}r_{iA}^{dC}({}_{n+1}\Delta\boldsymbol{d}^C, {}_{n+1}\Delta\varphi^C) \equiv M_{ijAB}\,{}_{n+1}\ddot{d}_{jB}^C + {}_{n+1}f_{iA}^{int} - {}_{n+1}f_{iA}^{ext} = 0 \\
&{}_{n+1}r_A^{\varphi C}({}_{n+1}\Delta\boldsymbol{d}^C, {}_{n+1}\Delta\varphi^C) \equiv {}_{n+1}f_A^{\varphi int} - {}_{n+1}f_A^{\varphi ext} = 0 \\
&{}_{n+1}d_{iA}^C = {}_{n+1}\overline{u}_{iA} \ \textit{on}\ \partial\Omega^u \\
&{}_{n+1}\varphi_A^C = {}_{n+1}\overline{\varphi}_A \ \textit{on}\ \partial\Omega^\varphi \\
&n \leftarrow n+1, \ \text{Go to the next load increment}
\end{aligned}
\tag{6.8}
$$

where ${}_{n+1}r_{iA}^{dC}$, ${}_{n+1}r_{iA}^{\varphi C}$ and ${}_{n+1}\Delta d_{iA}^C$, ${}_{n+1}\Delta\varphi_A^C$ are the coarse-scale residuals, displacement and potential increments in the $(n+1)^{\text{th}}$ load increment, respectively, and

$$
M_{ijAB} = \delta_{ij}\int_\Omega \rho_M^C N_A^C N_B^C d\Omega, \tag{6.9}
$$

$$
f_{iA}^{int} = \int_\Omega \frac{\partial N_A^C}{\partial X_J}K_{iJ}^C d\Omega, \tag{6.10}
$$

$$
f_{iA}^{ext} = \int_\Omega N_A^C B_i^C d\Omega + \int_{\partial\Omega^T} N_A^C \overline{T}_i \, d\Gamma, \tag{6.11}
$$

$$
f_A^{\varphi int} = \int_\Omega \frac{\partial N_A^C}{\partial X_J}\mathcal{D}_J^C d\Omega, \tag{6.12}
$$

$$
f_A^{\varphi ext} = \int_\Omega N_A^C \rho_E^C d\Omega + \int_{\partial\Omega^\omega} N_A^0 \overline{\omega} d\Gamma, \tag{6.13}
$$

where $M_{ijAB}$ is the mass, $f_{iA}^{int}$ and $f_{iA}^{ext}$ the internal and external forces, respectively. It is again convenient to express the coarse-scale governing equations in the deformed configuration

$$M_{ijAB} = \delta_{ij}\int_{\Omega_x} \rho_m^C N_A^C N_B^C d\Omega_x, \tag{6.14}$$

$$f_{iA}^{int} = \int_{\Omega_x} \frac{\partial N_A^C}{\partial x_j}\sigma_{ij}^C d\Omega_x, \tag{6.15}$$

$$f_{iA}^{ext} = \int_{\Omega_x} N_A^C b_i^C d\Omega_x + \int_{\partial\Omega_x^t} N_A^C \overline{t}_i d\Gamma_x, \tag{6.16}$$

$$f_A^{\varphi int} = \int_{\Omega_x} \frac{\partial N_A^C}{\partial x_j} D_j^C d\Omega_x, \tag{6.17}$$

$$f_A^{\varphi ext} = \int_{\Omega_x} N_A^C \rho_e^C d\Omega_x + \int_{\partial\Omega_x^\varpi} N_A^C \overline{\varpi}_c d\Gamma_x, \tag{6.18}$$

where

$$\rho_m^C = \rho_M^C / J^C, \qquad b_i^C = B_i^C / J^C, \quad \rho_e^C = \rho_E^C / J^C, \qquad \overline{t}_i d\Gamma_x = \overline{T}_i d\Gamma, \ \overline{\varpi}_x d\Gamma_x = \overline{\varpi} d\Gamma, \tag{6.19}$$

$$\sigma_{ij}^C = F_{jK}^C K_{iK}^C / J^C \tag{6.20}$$

and $J^C$ is the determinant of $F_{iJ}^C$; $\Omega_x$, $d\Omega_x, \partial\Omega_x, d\Gamma_x$ denote volume, infinitesimal volume, boundary and surface element in the current configuration.

We now focus on deriving a closed form expression for the overall Cauchy stress $\sigma_{ij}^C$ and electric displacement $D_j^C$. Substituting (6.6) into (3.37), (3.38) and recalling $d\Theta_y = Jd\Theta_Y$, we have

$$\begin{aligned} K_{iK}^C(\hat{\boldsymbol{X}}, t) &= \frac{1}{|\Theta_Y|}\int_{\Theta_y} F_{Km}^{-1}\sigma_{im} d\Theta_y, \\ \mathcal{D}_K^C(\hat{\boldsymbol{X}}, t) &= \frac{1}{|\Theta_Y|}\int_{\Theta_y} F_{Km}^{-1} D_m d\Theta_y. \end{aligned} \tag{6.21}$$

Inserting (6.21) into (6.20) and denoting the volume of the coarse-scale (intermediate) configuration as $|\Theta_y^*| = \overline{J}|\Theta_Y|$, the overall quantities can be expressed as

$$\boxed{\begin{aligned}\sigma_{ji}^{C} &= \frac{1}{\left|\Theta_y^*\right|}\int_{\Theta_y} \Delta F_{jm}^{-1}\sigma_{mi}\, d\Theta_y \\ D_j^{C} &= \frac{1}{\left|\Theta_y^*\right|}\int_{\Theta_y} \Delta F_{jm}^{-1} D_m\, d\Theta_y\end{aligned}} \tag{6.22}$$

where $\Delta F_{jm}^{-1} = F_{jK}^{C} F_{Km}^{-1}$ maps the fine-scale deformed configuration $\Theta_y$ into the coarse-scale deformed configuration $\Theta_y^*$ as illustrated in Figure 6.

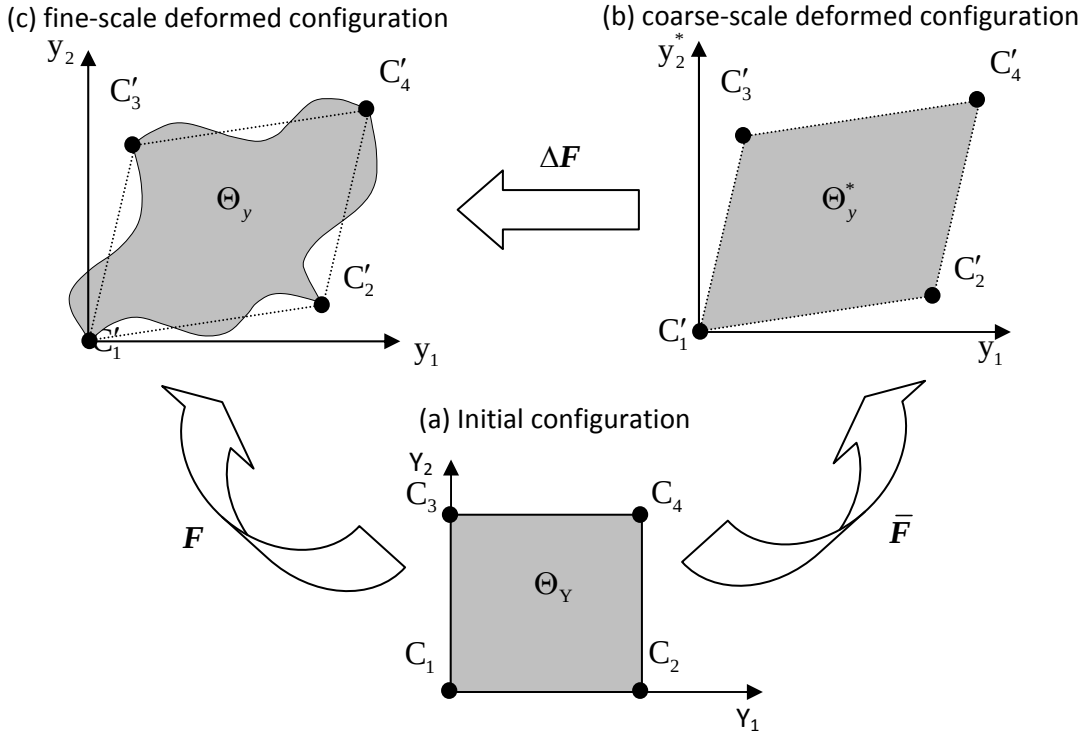


Figure 6: Unit cell configurations: (a) initial, (b) coarse-scale (intermediate), (c) fine-scale deformed (final)

The coarse-scale problem may be solved using either explicit or implicit time integration [87].

## 7. Numerical examples

In this section we will consider a numerical example illustrating the ability of the mathematical homogenization to resolve the coarse-scale behavior of heterogeneous materials with nonlinear electromechanical coupling subjected to electric field. The results of the mathematical homogenization (to be referred as MH) will be compared to the direct numeric simulation (DNS)

where a very fine mesh is employed to resolve fine-scale details. For simplicity, we will consider two-dimensional problem (plane strain).

For nonlinear electromechanical material we will use a simple relaxor ferroelectric material model proposed in [50], where polarization and strain are used as independent variables. It is assumed that material is isotropic, where the stress depends linearly on total strain. The polarization induced strain $\varepsilon_E$ depends on the square of polarization, i.e., it is electrostrictive material, where polarizations saturates to $P_S$ at high electric fields. The internal energy function for relaxor ferroelectric was proposed by Hom and Shankar as

$$U = \frac{1}{2}\left(\boldsymbol{\varepsilon} - \boldsymbol{\varepsilon}_E\right) : \mathbf{C} : \left(\boldsymbol{\varepsilon} - \boldsymbol{\varepsilon}_E\right) + \frac{1}{2k}\left[ |\mathbf{P}| \ln\left(\frac{P_s + |\mathbf{P}|}{P_s - |\mathbf{P}|}\right) + P_s \ln\left(1 - \left(\frac{|\mathbf{P}|}{P_s}\right)^2\right)\right], \tag{7.1}$$

$\varepsilon_E$ is polarization-induced strain defined as

$$\varepsilon_E = \mathbf{Q} : (\mathbf{PP}) = \left(Q_{11} - Q_{12}\right)\mathbf{PP} + Q_{12}|\mathbf{P}|^2\,\mathbf{I}, \tag{7.2}$$

$\mathbf{C}$ and $\mathbf{Q}$ are an isotropic elastic stiffness matrix and an isotropic electrostrictive strain coefficient matrix; $k$ is material constant; coefficients $Q_{11}$ and $Q_{12}$ are defined so that the longitudinal and transverse induced strains relative to polarization direction are $Q_{11}|\mathbf{P}|^2$ and $Q_{12}|\mathbf{P}|^2$, respectively.

Stress and electric field are calculated from the internal energy by differentiation

$$\boldsymbol{\sigma} = \frac{\partial U}{\partial \boldsymbol{\varepsilon}} = \mathbf{C} : \left(\varepsilon - \mathbf{Q} : (\mathbf{PP})\right), \tag{7.3}$$

$$\mathbf{E} = \frac{\partial U}{\partial \mathbf{P}} = -2\left(\varepsilon - \mathbf{Q} : (\mathbf{PP})\right) : \mathbf{C} : \mathbf{Q} \cdot \mathbf{P} + \frac{1}{k}\operatorname{arctanh}\left(\frac{|\mathbf{P}|}{P_S}\right)\frac{\mathbf{P}}{|\mathbf{P}|}. \tag{7.4}$$

The first term in (7.4) represents the converse electrostrictive effect, while the second term represents the stress-free dielectric behavior. Polarization can be written in more compact form as

$$\mathbf{P} = P_S \tanh\left(k|\mathbf{R}|\right)\frac{\mathbf{R}}{|\mathbf{R}|}, \tag{7.5}$$

where

$$\mathbf{R} = \mathbf{E} + 2\left(\boldsymbol{\varepsilon} - \mathbf{Q} : (\mathbf{PP})\right) : \mathbf{C} : \mathbf{Q} \cdot \mathbf{P} = \mathbf{E} + 2\boldsymbol{\sigma} : \mathbf{Q} \cdot \mathbf{P}. \tag{7.6}$$

For a given strain and electric field (which are known from the previous iteration), one can solve (7.5) for induced polarization and then use (7.3) to calculate stress. The Jacobian for the constitutive model can be derived from (7.5) and (7.3) as

$$\begin{bmatrix} d\boldsymbol{\sigma} \\ d\mathbf{P} \end{bmatrix} = \begin{bmatrix} \mathbf{C} - 4\mathbf{C}:\mathbf{Q}\cdot\mathbf{P}\cdot\mathbf{Z}\cdot(\mathbf{Q}\cdot\mathbf{P})^T:\mathbf{C} & -2\mathbf{C}:\mathbf{Q}\cdot\mathbf{P}\cdot\mathbf{Z} \\ 2\mathbf{Z}\cdot(\mathbf{Q}\cdot\mathbf{P})^T:\mathbf{C} & \mathbf{Z} \end{bmatrix} \cdot \begin{bmatrix} d\boldsymbol{\varepsilon} \\ d\mathbf{E} \end{bmatrix}, \tag{7.7}$$

where

$$\mathbf{Z} = \left[\mathbf{I} - \mathbf{H}\cdot\left[2\left(\boldsymbol{\varepsilon} - \mathbf{Q}:(\mathbf{PP})\right):\mathbf{C}:\mathbf{Q} - 4(\mathbf{Q}\cdot\mathbf{P})^T:\mathbf{C}:\mathbf{Q}\cdot\mathbf{P}\right]\right]^{-1}\cdot\mathbf{H} \tag{7.8}$$

and

$$\mathbf{H} = P_s \tanh\left(k|\mathbf{R}|\right)\left[\frac{\mathbf{I}}{|\mathbf{R}|} - \frac{\mathbf{RR}}{|\mathbf{R}|^3}\right] + \frac{kP_s\mathbf{RR}}{\cosh^2\left(k|\mathbf{R}|\right)|\mathbf{R}|^2}. \tag{7.9}$$

| Y(GPa) | ν | $Q_{11}(m^4/C^2)$ | $Q_{12}(m^4/C^2)$ | $Ps(C/m^2)$ | k(m/MV) |
|---|---|---|---|---|---|
| 115 | 0.26 | $1.33^x10^{-2}$ | $-6.06^x10^{-3}$ | 0.2589 | 1.16 |

Table 1. Model parameters for PMN-PT-BT at 5°C

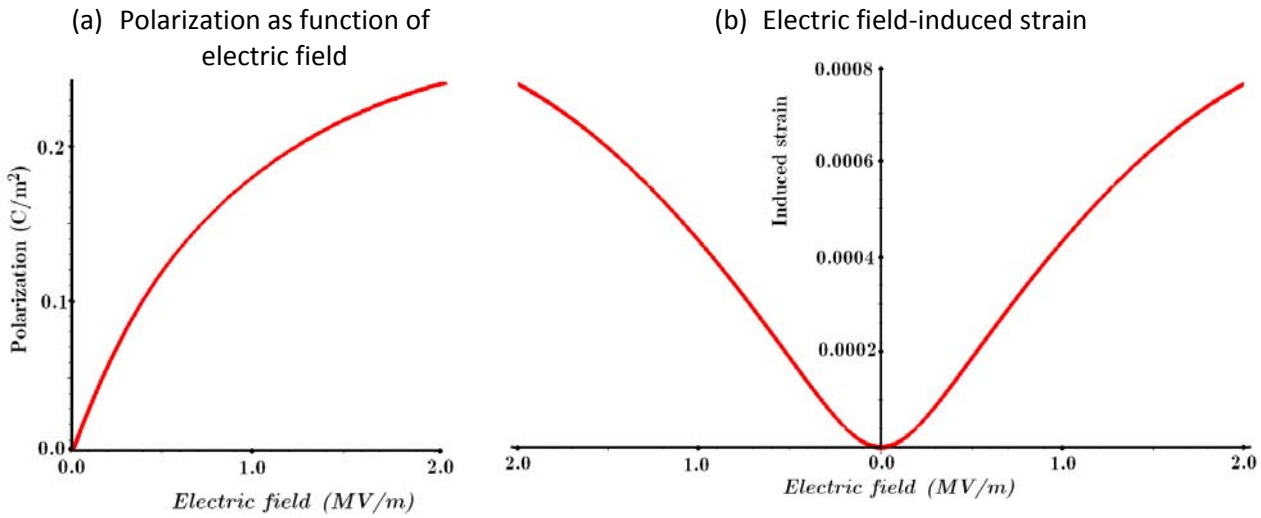


Figure 7. Electrostrictive material model

Numerical values of model parameters for PMN-PT-BT at 5°C are given in Table 1. Dependence of polarization and induced strain on electric field is presented in Figure 7.

The above model is valid for small strains, so consequently we consider a problem where induced strains are small, in which case stress, strain, electric displacement and electric field coincide in initial and deformed configurations.

7.1 Actuator example

This example demonstrates the ability of mathematical homogenization to model the dependence of coarse-scale behavior on fine-scale details.

Consider a beam with top half made of electroactive material and lower half made of material with no electromechanical coupling (Figure 8). The electroactive material is a periodic composite with unit cell consisting of matrix material and horizontal electroactive fiber. Both materials have the same mechanical properties (linear isotropic material with Young modulus $E$ and Poisson ratio $\nu$ ), with fiber additionally having electromechanical coupling – electrostriction with parameters given in Table 1. Unit cell dimensions are 100x100.

The left side of the beam is mechanically fixed and grounded. A potential 36GV is applied to the right hand side of the beam.

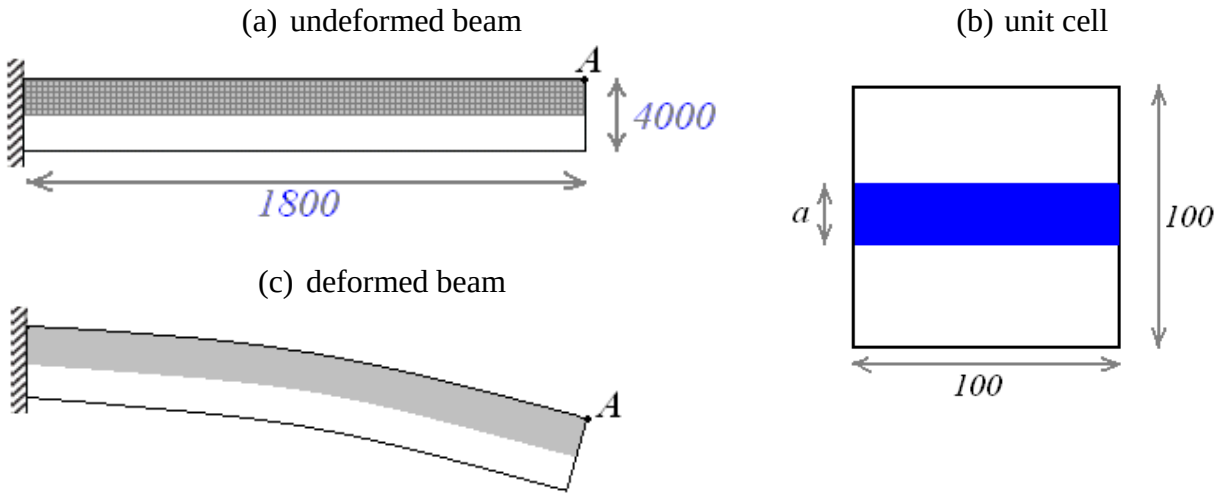


Figure 8: a) geometry of the beam and boundary conditions: the upper half is made of heterogeneous material, containing electroactive phase and phase without electromechanical coupling and consisting of periodic repetition of unit cells, b) a unit cell consisting of matrix and electrostrictive horizontal fiber, c) deformation of the beam when voltage is applied to the right side

When voltage is applied, the electrostrictive material in the upper half of the beam extends due to electrostriction effect and the beam will bend as shown on figure 8.c. This permits using the beam as an actuator.

We considered three cases with different fiber thicknesses (diameter in 3D) a: $a$=100 (i.e. the whole unit cell consists of electrostrictive material), $a$=60 and $a$=40. The deflections of the point A for different fiber thicknesses $a$ found by DNS-simulation are shown in Figure 9.a. It can be seen that different fiber sizes result in different actuation capabilities for the same loading, i.e., coarse-scale response is sensitive to the fine-scale details.

(a) (b)

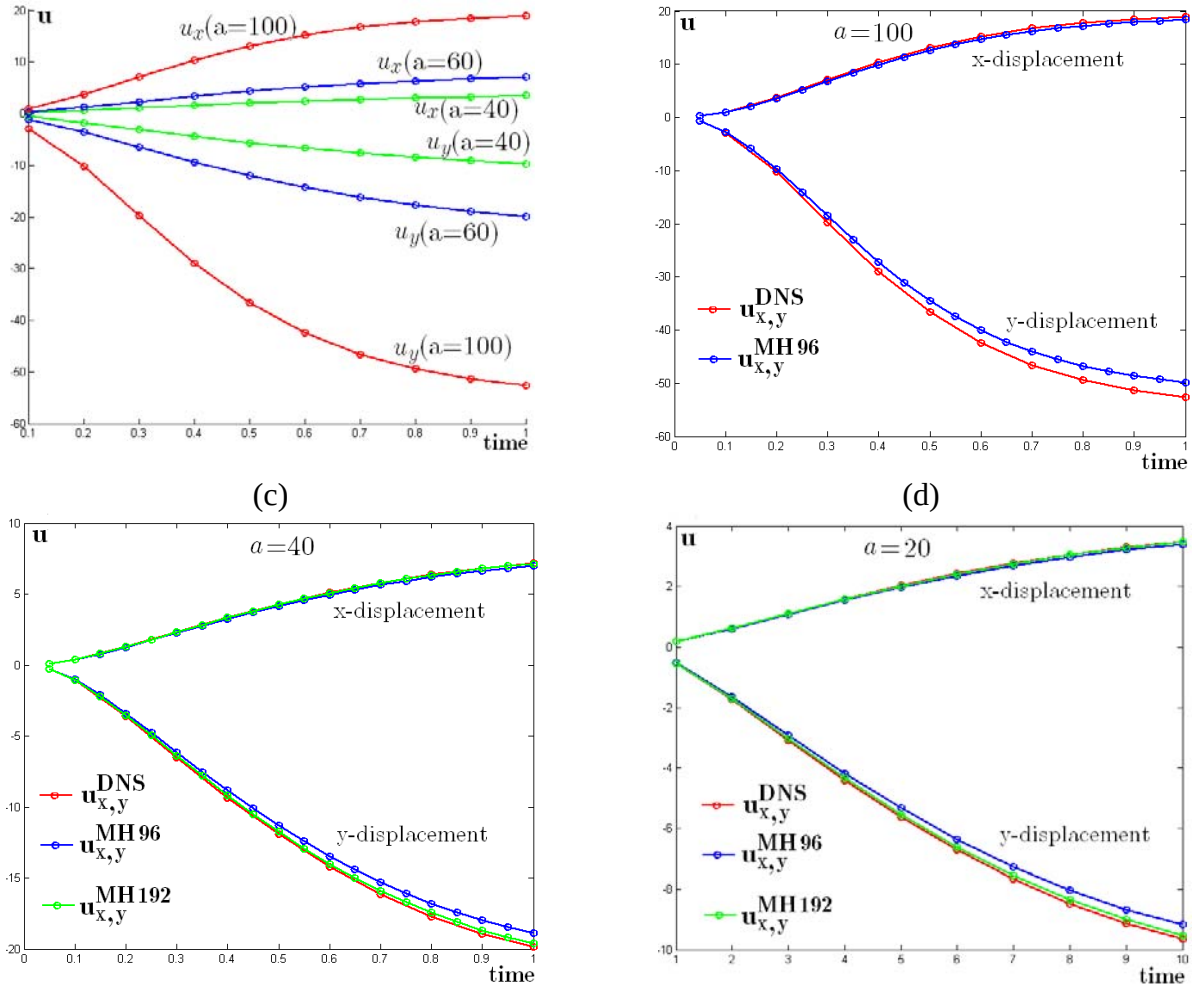


Figure 9: (a) displacements of point A, DNS simulations of actuation with different fractions of electrostrictive phase and Comparison of DNS (red line) and MH (blue line for 96 element and green line for 192 elements) solutions, for different thicknesses of electroactive fiber b) $a$=100, c)$a$=40 d) $a$=20.

The purpose of homogenization is to capture this dependence. Figure 9 shows also the comparison of DNS simulation with MH for different values of $a$. The MH simulations were performed for two different meshes with 96 elements and with 192 elements to study the convergence of MH solution to DNS solution. For $a$=20, the error between DNS and MH was 4.8% for 96 element mesh and 1.3% for 192 element mesh. For $a$=40, the error was 4.9% and 1.4%, respectively. For $a$=100, error was 5%. These results suggest that the mathematical homogenization is capable of reproducing the reference solution and captures the dependence of the coarse-scale response on fine-scale details.

7.2 Beam bending

Now consider the whole beam made of an electrostrictive material subjected to a linearly varying traction $F = 0.25 \cdot 10E + 5 \cdot Y$ Pa, as shown in Figure 10. The left side of the beam is mechanically

fixed and grounded. Electric potential $\varphi$ is applied to the right hand side of the beam. Again, the unit cell consists of matrix and fiber as depicted in Figure 8.b. with $a$=40. The matrix is assumed to be hyperelastic material with stress depending exponentially on the first invariant of the strain $I_1 = \varepsilon_{11} + \varepsilon_{22}$.


Figure 10. Beam with mechanical load applied to the left end.

The application of electric field changes the mechanical properties of the beam which results in different deflections under the same loading. We compare the results of DNS and MH to show the ability of MH to capture the change of mechanical properties due to biasing fields.

Figure 11 shows the deflection of point A for the two cases. In the first case the applied potential was $\varphi$=36GV. The result of DNS simulation is depicted by red line and MH (192 elements) simulation is depicted with a green line. The difference between DNS and MH at time t=0.5 was 5.6% for 96 elements and 1.6% for 192 elements. In the second case the right end of the beam was grounded, $\varphi$=0. The result of DNS simulation is depicted by blue line and MH (192 elements) simulation is depicted by magenta line. The difference between DNS and MH simulation at time t=0.5 was 5.2% for 96 elements and 1.5% for 192 elements.

It can be seen that the mathematical homogenization is capable of capturing the change of mechanical properties due to biasing electric fields and reproduces the reference solution with good approximation.

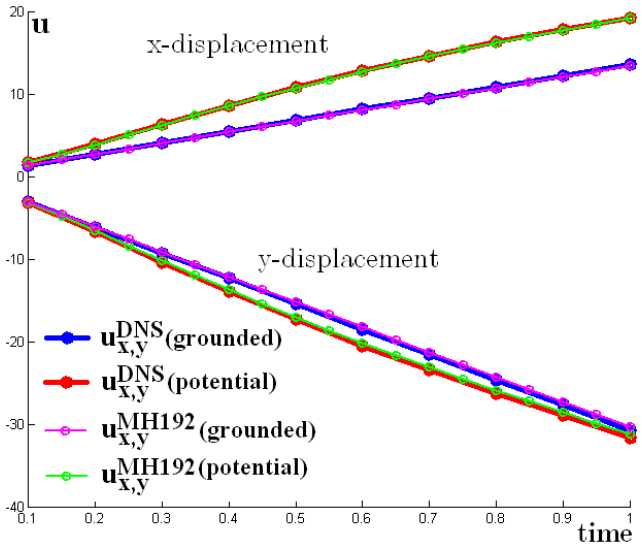


Figure 11. Comparison the DNS and MH simulations for beam bending.

## 8. Conclusions and future work

The examples considered in this manuscript show that nonlinear mathematical homogenization captures well the coarse-scale behavior of heterogeneous electroactive composite and its dependence on the fine-scale details.

At the same time the method shares the shortcomings common to the first order homogenization methods; it is insensitive to the absolute size of the UC because of assumption of UC infinitesimality [81]. This lack of accuracy increases with the unit cell size and the magnitude of strains and electric fields inhomogeneities.

In future we plan to study mathematical homogenization for various dynamic problems. In particular of interest are studies of wave propagation in the media with periodic resonant structures. It would be interesting to explore if mathematical homogenization can capture the negative effective refractive indexes as it was found in metamaterials. Can this framework be used to control bandgaps by biasing fields and will it allow extending effective bandgaps for use in various devices (for subwavelength imaging, wave attenuation etc). The other interesting phenomenon, which possibly may be studied using mathematical homogenization is the controlled response of smart structures to various impacts. Depending on the impact a control strategy may be developed to obtain the desired response from the smart structure. This phenomenon might be utilized in development of smart armor and other structures. Fine-scale structure optimization aimed at optimizing coarse-scale properties, in particular for electroactive polymers containing composites, is another useful application of the method. The asymptotic expansion would allow to

isolate the term $\varphi^1\left(\hat{\mathbf{X}}, \mathbf{Y}, t\right)$, responsible for electrostrictive and electrostatic coupling. Making this term larger will permit increasing the actuation.


## Acknowledgement

The authors wish to thank Dr. Peter Chung and LaMattina for supporting this work.


## 9. References


1 M.J. Buehler, B.P. Betting, G.G. Parker, Numerical homogenization of active material finite-element cells. Communications in Numerical Methods in Engineering 19, pp. 977-989, 2003

2 M. Buehler, B. Bettig, G. Parker Topology optimization of smart structures using a homogenization approach. SPIE's 9th Annual International Symposium on Smart Structures and Materials, San Diego, 2002.

3 Sigmund O, Torquato S. Design of smart composite materials using topology optimization. Smart Material Structures 1999; 8:365–379

4 Gabbert U, Weber C-T. Optimization of piezoelectric material distribution in smart structures. Proceedings, SPIE Conference on Mathematics and Control in Smart Structures, Newport Beach, CA, Vol. 3667, 1999; 13–22

5 Silva E, Fonseca J, Kikuchi N. Optimal design of periodic piezocomposites. Computer Methods in Applied Mechanics and Engineering 1998; 159(2):49–77

6 Mijar A, Swan C, Arora J, Kosaka I. Continuum topology optimization for concrete design of frame bracing structures. Journal of Structural Engineering (ASCE) 1998; 124:541–500

7 Buehler M. Homogenization of smart material cells for topological optimization. Master's Thesis, Michigan Technological University, 2001

8 Y. Uetsuji, Y. Nakamura, et al Numerical investigation on ferroelectric properties of piezoelectric materials using a crystallographic homogenization method. Modeling and Simulation in Materials Science and Engineering, 12, pp. 303-317, 2003

9 J. Li, C.T. Chan, Double Negative acoustic metamaterial, Phys. Rev. E, 70, 055602-1, 2004

10 Z. Liu, X. Zhang, Y. Mao, Y. Y. Zhu, Z. Yang, C.T. Chan, P. Sheng Locally resonant sonic metamaterials, Science, 289,17341736, (2000) DOI: 10.1126/science.289.5485.1734

11 S. Guenneau, A. Movchan, G. Petursson, S. A. Ramakrishna, Acoustic metamaterials for sound focusing and confinement New Journal of Physics 9,1-15, (2007) 399 PII: S1367-2630(07)45305-8

12 M. Gorkunov, M.Lapine, E. Shamonina, K.H. Ringhofer, Effective magnetic properties of a composite material with circular conductive elements, Eur. Phys. J. B 28, 263-269, (2002)

13 E.N. Economou, Th. Koschny, C.M. Soukoulis Strong magnetic response of metamaterials, Phys. Rev. B 77, (2008)

14 J. Yang, An introduction to the theory of piezoelectricity Springer 2005

15 . P. Sorokin, P. P. Turchin, S. I. Burkov, D. A. Glushkov and K. S. Alexandrov, Influence of static electric field, mechanical pressure and temperature on the propagation of acoustic waves in $La_3Ga_5SiO_{14}$ piezoelectric single crystals, in: *Proc. IEEE Int. Frequency Control Symp.*, 1996, pp. 161-169.

16 C.N. Della, D. Shu, Effective properties of 1-3 piezoelectric composites: effect of polarization orientation. International conference on smart Materials and Nanotechnology in Engineering edited by Shanyi Du, Jinsong Leng, Anand K. Asundi. Proc of SPIE Vol. 6423, 642323 1-7, 2007

17 Bar-Cohen, Y., "Actuation of biological inspired intelligent robotics using artificial muscles," *Industrial Robot*, **4**, 331–337 (2003).

18 Bar-Cohen, Y., EAP history, current status, and infrastructure, in Y. Bar-Cohen (ed.), Electroactive Polymer (EAP) Actuators as Artificial Muscles, chap. 1, pp. 3–44, SPIE press, Bellingham, WA, 2001.
19 Zhang, Q. M., and Scheinbeim, J., Electric EAP, in Y. Bar-Cohen (ed.), Electroactive Polymer (EAP) Actuators as Artificial Muscles, chap. 4, pp. 89–120. SPIE press, Bellingham, WA, 2001.
20 D.L. DeVoe,A. P. Pisano, Modelling and optimal design of piezoelectric cantilever microactuators *J. Microelectromech. Syst.* **6** 266–70, 1997
21 J. Scott, Applications of modern ferroelectrics, science, vol. 315, 2007, 954-959
22 J.F. Scot Nanoferroelectrics: statics and dynamics, J. Phys. Condens. Matter 18(2006), R361-R386
23 A.Pimpin, Y. Suzuki, N. Kasagi, MICRO ELECTROSTRICTIVE ACTUATOR WITH METAL COMPLIANT ELECTRODES FOR FLOW CONTROL APPLICATIONS, 17th IEEE Int. Conf. MEMS 2004, Maastricht, (2004), pp.478-481
24 A. G. Shard, V. R. Dhanaka, A. D. Smith, An electrostrictive drive for fine pitch control in double-crystal monochromators, J. Synchrotron Rad. (1998). 5, 829-831
25 R. Suyama, K. Tanemoto, Y. Kobayashi, Autofocusing system of optical microscope utilizing electrostrictive actuators, Japanese Journal of Applied Physics, vol.30, no. 6, June, 1991, pp. 1290-1294
26 G. deBotton, L.Tevet-Dereee, E.A. Socolsky Electroactive heterogeneous polymers: Analysis and applications to laminated composites, Mechanics of advanced materials and structures, 14, 13-22, 2007
27 H.W. Joo, C.H. Lee, J.S. Rho, H.K. Jung Identification of material constants for piezoelectric transformers by three-dimensional, finite-element method and a design-sensitivity method, IEEE transactions on ultrasonics, ferroelectrics and frequency control, vol. 50, no. 8., 2003, 965-971
28 P. Brochu, Q.Pei, Advances in dielectric elastomers for actuators for Artificial Muscles, Macromolecular Rapid CommunicationsVolume 31, Issue 1, 2010
29 F. Carpi, D. De Rossi, R. Kornbluh, R. Pelrine, and P. Sommer-Larsen, Dielectric Elastomers as Electromechanical
Transducers (Elsevier, Oxford, 2008).
30 G. Kovacs, L. During, S. Michel, G. Terrasi, Stacked dielectric elastomer actuator for tensile force transmission, Sensors and Actuators A: Physical, vol 155, Issue 2, Pages 299-307, 2009
31 I. Anderson, T. Hale, T. Gisby, T. Inamura, T. McKay, B. O'Brien, S. Walbran, E. Calius, A thin membrane artificial muscle rotary motor, Appl Phys A (2010) 98: 75–83, DOI 10.1007/s00339-009-5434-5
32 Zhang, Q. M., Li, H., Poh, M., Xia, F., Cheng, Z.-Y., Xu, H., and Huang, C.,"An all-organic composite actuator material with a high dielectric constant,"*Nature* **419**, 284–289 (2002).
33 Huang, C., Zhang, Q. M., deBotton, G., and Bhattacharya, K., "Allorganic dielectric-percolative three-component composite materials with high electromechanical response," *Applied Physics Letters* **84**, 4391–4393 (2004).
34 Huang C., and Zhang, Q. M., "Enhanced dielectric and electromechanical responses in high dielectric constant all-polymer percolative composites," *Adv. Func. Mater.* **14**, 501–506 (2004).
35 Li, J. Y., Huang, C., and Zhang, Q. M., "Enhanced electromechanical properties in all-polymer percolative composites," *Applied Physics Letters* **84**, 3124–3126 (2004).
36 X. Zhao, Z. Suo Theory of dielectric elastomers capable if giant deformation of actuation, Phys Rev Let 2010
37 H. F. Tiersten, On the nonlinear equations of thermoelectroelasticity, *Int. J. Engng Sci.*, 9, 587-604, 1971
38 Toupin, R. A., "The elastic dielectric," *Arch. Rational. Mech. Anal.* **5**, 849–915 (1956).
39 A. Dorfmann, R. W. Ogden, Nonlinear electroelasticity, Acta Mechanica 174, 167–183 (2005) DOI 10.1007/s00707-004-0202-2
40 D.K. Vu, P. Steinmann, Nonlinear electro- and magneto-elastostatics: Material and spatial settings, International Journal of Solids and Structures 44 (2007) 7891–7905
41 D. F. Nelson, Theory of nonlinear electroacoustics of dielectric, piezoelectric, and pyroelectric crystals, J. Acoust. Sec. Am., VoL 63, No. 6, June 1978
42 F. Bampi, A. Morro, a Lagrangian density for the dynamics of elastic dielectric, Int. J. Non-Linear Mechanics, vol. 18, 6, 441-447, 1983

43 R. McMeeking, C. M. Landis, S.M.A. Jimenez, Aprinciple of virtualwork for combined electrostatic and mechanical loading of materials, International Journal of Non-Linear Mechanics 42 (2007) 831 – 838
44 D. K. Vu,P.Steinmann, Theoretical and numerical aspects of the material and spatial settings in nonlinear electro-elastostatics, Int J Fract (2007) 147:109–116, DOI 10.1007/s10704-007-9141-y
45 Y.H. Pao, Electromagnetic forces in deformable continua, in: S. Nemat-Nasser (Ed.), Mechanics Today, vol. 4, Pergamon Press, NewYork, 1978, pp. 209–305
46 G.A. Maugin, Continuum Mechanics of Electromagnetic Solids, North-Holland, Amsterdam, 1988
47 A.C. Eringen, G.A. Maugin, Electrodynamics of Continua I Foundations and Solid Media & II Fluids and Complex Media, Springer, New York,1990.
48 H.F. Tiersten, A Development of the Equations of Electromagnetism in Material Continua, Springer, New York, 1990. A.
49 Kovetz, The Principles of Electromagnetic Theory, Cambridge University Press, Cambridge, 1990.
50 C.L. Hom, N. Shankar, A finite element method for electrostrictive ceramic devices. Int. J. Solids Structures 33(12), pp. 1757-1779, 1996
51 E.B. Tadmor, U.V. Waghmare, G.S. Smith, E. Kaxiras Polarization switching in $PbTiO_3$: an Ab Initio Finite element Simulation, Acta Materialia, 50, 2989-3002(2002).
52 A.M. Bratkovsky, A.P. Levanyuk, Depolarizing field and “real” hysteresis loops in nanometer-scale ferroelectric films, Applied Physics Letters, 89, 253108
53 G. Nagai, T. Hayashi, T. Takekawa, Numerical procedure for polycrystalline ferroelectric/Ferroelastic problems using Landau’s phenomenological model, Journal of Solid Mechanics and Materials Engineering, vol. 2, No. 10, 1307-1317, 2008
54 F.X. Li, R.K.N.D. Rajapaske, Nonlinear finite element modeling of polycrystalline ferroelectric based on constrained domain switching, Computational Material Science, 44, (2008), 322-329
55 A.W. Richards, G.M. Odegard, Constitutive modeling of electrostrictive Polymers using a Hyperelasticity-Based Approach, Journal of Applied Mechanics, Vol. 77, No. 1, 014502 (2010)
56 Mahut T, Agbossou A, Pastor J. Dynamic analysis of piezoelectric fiber composite in an active beam using homogenization and finite element methods, Journal of Intelligent Material Systems and Structures 1998,vol. 9, no. 12,1009–1016.
57 Telega J, Galka A, Gambin B. Piezoelectricity and homogenization, application in biomechanics. Archieves ofMechanics 1991; 2:220–229.
58 Galka A, Telega J, Wojnar R. Homogenization and thermopiezoelectricity. Mechanics Research Communications1992; 19(4):315–324.
59 H. Berger, U. Gabbert et al, Finite element and asymptotic homogenization methods applied to smart composite materials. Computational mechanics, 33, pp. 61-67, 2003
60 A.C. Dent, C.R. Bowen et al, Effective properties for unpoled barium titanate. Journal of European Ceramic society, 27, pp. 3739-3743, 2007
61 B. Miara, E. Rohan et al, Application of multy-scale modeling to some elastic, piezoelectric and electromagnetic composites. Mechanics of advanced materials and structures, 13, pp. 33-42, 2006
62 E. Lenglet, A.-C. Hladky-Hennion, J.-C. Debus, Numerical homogenization techniques applied to piezoelectric composites. J. Acoust. Soc. Am., 113(2), pp. 826-833, 2002
63 C.N. Della, D. Shu, Effective properties of 1-3 piezoelectric composites: effect of polarization orientation, International conference on Smart Materials and Nanotechnology in Engineering edited by S. Du, J. Leng, A. K. Asundi, Proc of SPIE vol. 6423, 642323, (2007)
64 Fish J, Shek KL. Finite deformation plasticity of composite structures: computational models and adaptive strategies. *Computer Methods in Applied Mechanics and Engineering* 1999; **172**:145–174.
65 J. Fish, R. Fan, Mathematical homogenization of nonperiodic heterogeneous media subjected to large deformation transient loading. International Journal for numerical methods in engineering, 76, 1044-1064, 2008
66 Yuan Z, Fish J. Towards realization of computational homogenization in practice. *International Journal for Numerical Methods in Engineering* 2008; **73**:361–380.

67 Clayton JD, Chung PW. An atomistic-to-continuum framework for nonlinear crystal mechanics based on asymptotic homogenization. *Journal of Mechanics and Physics of Solids* 2006; **54**: 1604–1639.
68 Ghosh S, Lee K, Moorthy S. Two scale analysis of heterogeneous elastic–plastic materials with asymptotic homogenization and Voronoi cell finite element model. *Computer Methods in Applied Mechanics and Engineering* 1996; **132**:63–116.
69 Kouznetsova V, Brekelmans W-A, Baaijens FP-T. An approach to micro–macro modeling of heterogeneous materials. *Computational Mechanics* 2001; **27**:37–48.
70 Terada K, Kikuchi N. Nonlinear homogenization method for practical applications. In C*omputational Methods in Micromechanics*, vol. AMD-212/MD-62, Ghosh S, Ostoja-Starzewski M (eds). ASME: New York, 1995; 1–16.
71 Terada K, Kikuchi N. A class of general algorithms for multi-scale analysis of heterogeneous media. *Computer Methods in Applied Mechanics and Engineering* 2001; **190**:5427–5464.
72 Li A, Li R, Fish J. Generalized mathematical homogenization: from theory to practice. *Computer Methods in Applied Mechanics and Engineering* 2008; **197**:3225–3248
73 L.D. Landau, E.M. Lifshitz, Statistical physics. Part I. (Course of theoretical physics; V.5), Pergamon Press, 1980
74 G. F. Smith, M. M. Smith and R. S. Rivlin, Integrity bases for a symmetric tensor and a vector-the crystal classes, *Arch. Rat. Mech. Anal.*, 12, 93-133, 1963
75 McMeeking, R. M. (1987). On mechanical stresses at cracks in dielectrics with application to dielectric breakdown. *J. Appl. Phys. 62,3*116-22
76 McMeeking, R. M. (1989). Electrostrictive stress near crack like flaws. J. Appl. Math. Phys. 40,615-627.
77 L.D. Landau, E.M. Lifshitz, Statistical physics. Part I. (Course of theoretical physics; V.5), Pergamon Press, 1960
78 D. Damjanovic, Ferroelectric, dielectric and piezoelectric properties of ferroelectric thin films and ceramics, Rep. Prog. Phys. 61 (1998) 1267-1324
79 R. E. Newham, 1990 Proc. Chemistry of Electronic Ceramic Materials (National Institute of Standards and technology, Jackson, WY) Special Publication 804
80 J. M. Guedes and N. Kikuchi, Preprocessing and postprocessing for materials based on the homogenization method with adaptive finite element methods, *Computer Methods in Applied Mechanics and Engineering*, Vol. 83, pp. 143-198, 1990
81 J. Fish, S. Kuznetsov, Computational Continua, Int, J. for Num. Methods in Engineering, vol. 84, 7, 774-802, 2010
82 A. Benssousan, J.L. Lions and G. Papanicoulau, “Asymptotic Analysis for Periodic Structures”, *North-Holland*, 1978
83 E. Sanchez-Palencia, “Non-homogeneous media and vibration theory,” Lecture notes in physics, Vol. 127, Springer-Verlag. Berlin. (1980)
84 N.S. Bakhvalov and G.P. Panassenko, Homogenization: Averaging Processes in Periodic Media, Kluwer Academic Publishers, 1989
85 G. Allaire, G. Bal, Homogenization of the criticality spectral equation in neutron transport, RAIRO – Modelisation mathematique et analyse numerique, tome 33, $n^0$4 (1999), p.721-746
86 S. D. Mesarovic and J. Padbidri, Minimal kinematic boundary conditions for simulations of disordered microstructures, Philosophical Magazine, Vol. 85, No. 1, pp. 65-78, (2005)
87 Belytschko T, Liu WK, Moran B. *Nonlinear Finite Elements for Continua and Structures*. Wiley: New York, 2000